A novel nonlinear isolated rooftop tuned mass damper-inerter (IR-TMDI) system for seismic response mitigation of buildings

Komal Rajana[1] and Agathoklis Giaralis[2]*

[1]PhD Candidate, City, University of London, Northampton Square, London EC1V 0HB, UK

[2]Associate Professor (Reader), City, University of London, Northampton Square, London EC1V 0HB, UK

*Corresponding author, E-mail: agathoklis.giaralis.1@city.ac.uk

Abstract

This paper conceptualizes a novel passive vibration control system comprising a tuned mass damper inerter (TMDI) contained within a seismically isolated rooftop and investigates numerically its effectiveness for seismic response mitigation of building structures. The working principle of the proposed isolated rooftop tuned mass damper inerter (IR-TMDI) system relies on the yielding of typical elastomeric isolators (e.g. lead rubber bearings) under severe earthquake ground motions to create a flexible rooftop which, in turn, increases the efficacy of the TMDI for seismic vibrations suppression. Herein, a nonlinear mechanical model is considered to explore the potential of IR-TMDI whereby the primary building structure is taken as linear damped single-mode system while the Bouc-Wen model is used to capture the nonlinear/hysteretic behavior of the rooftop isolators. An equivalent linear system (ELS), derived through statistical linearization, is used to expedite the optimal IR-TMDI tuning for different isolated rooftop properties, inertance, and primary structure natural periods under white noise excitations with different intensities as well as Kanai-Tajimi excitations for different soil conditions. It is found that tuning for maximizing TMDI seismic energy dissipation is more advantageous than tuning for minimizing primary structure displacement or acceleration response since it lowers deflection and force demands to the isolators and to the inerter. Further, significant primary structure displacement and acceleration reductions are achieved as the effective rooftop flexibility increases through reduction of the nominal strength of the isolators, which verifies the intended working principle of the IR-TMDI. This is also confirmed through response history analyses to the nonlinear model under four benchmark recorded ground motions. Moreover, for IR-TMDI with sufficiently flexible isolators, improved seismic structural performance with concurrent reduced deflection and force demands at the isolators is shown for all considered stationary excitations as the inertance scales-up, which is readily achievable technologically. Thus, it is concluded that the IR-TMDI mitigates effectively structural seismic response without requiring the inerter to span several floors, as suggested in previous studies, thus extending the TMDI applicability to both existing and low-rise new-built structures.

Keywords

Tuned mass damper inerter, floor isolation, Bouc-Wen model, statistical linearization, optimal energy design

1 Introduction and motivation

Over the past decades, various passive vibration control approaches for seismic structural response modification and energy dissipation have been considered in the scientific literature and in practice for improving the performance of buildings under earthquakes (e.g. Freddi et al. 2021). Common approaches involve the insertion of a laterally flexible (isolation) layer comprising elastomeric and/or sliding bearings at the basement of buildings (Naeim & Kelly 1999, Warn & Ryan 2012) or at an intermediate floor (Ryan & Earl 2010, Faiella & Mele 2020). The isolation layer elongates the fundamental structural natural period while enabling local seismic energy dissipation through nonlinear (hysteretic) behavior of the isolators. Both of these considerations reduce the total lateral seismic loads. Further, the isolation layer changes the shape of the first (dominant) mode of vibration which reduce interstorey drifts and floor accelerations throughout the building by localizing lateral seismic deflection demands at the isolators. Other approaches consider various damping devices such as viscous dampers (Berquist et al. 2019) and hysteretic dampers (Xie 2005) diffused throughout buildings as standalone struts to resist earthquake loads through increased seismic energy dissipation (Whittle et al. 2012), or placed at the isolation layer to increase energy dissipation in isolated buildings (Wolff et al. 2015), or incorporated within tuned mass dampers (TMDs) (Soto & Adeli 2013, Elias & Matsagar 2017). The latter approach, of particular interest to this work, relies on attaching a free-to-oscillate (secondary) mass to the top floor of the building (primary) structure via viscous dampers and stiffeners which are designed/tuned to minimize the seismic response of the building primary structure, dominated by the first mode of vibration (e.g. Rana & Soong 1998). TMDs may be implemented either as a hanging heavy-weight pendulum from the top floor (Zemp et al. 2011, Li et al. 2011) or by isolating the top floor (Villaverde 2002, Matta & De Stefano 2009) whereby the mass of the rooftop slab becomes the TMD secondary mass while the isolators are appropriately dimensioned such that the effective period of the isolated rooftop is tuned (i.e. matches closely) the fundamental frequency of the remaining building. They may have linear viscoelastic, non-linear elastic, or even hysteretic behavior in which case they oftentimes termed nonlinear energy sinks (Vakakis & Gendelman 2001, Tsiatas et al 2020).

Out of the different approaches discussed above, TMDs are the least considered in practice for the seismic protection of buildings, although they are widely used for mitigating wind-borne oscillations in slender/tall structures (Elias & Matsagar 2017, Colherinhas et al 2021). This is because TMDs require excessively large secondary mass for the effective mitigation of earthquake-induced oscillations corresponding to more than 15% of the building/structural mass (see e.g. De Angelis et al 2011 and therein references). To this end, in recent years, the tuned mass damper inerter (TMDI) configuration proposed by Marian and Giaralis (2013, 2014) has been widely considered in the literature for the seismic response mitigation of non-isolated buildings (Giaralis & Taflanidis 2018, Ruiz et al. 2018, Taflanidis et al. 2019, Kaveh et al. 2020, Patsialis et al. 2021, Djerouni et al. 2022) as it significantly relaxes the requirement for a large secondary mass. This is achieved by coupling a conventional top-floor TMD with an inerter device which links/supports the secondary mass to an intermediate floor, different from the top floor, thus resulting in a device assembly attached to two different building floors. The inerter is a mechanical element that produces a relative acceleration- dependent force proportional to a so-called inertance property measured in mass units (kg) (Smith 2002). Importantly, inertance scales-up practically independently from the inerter physical mass using mechanical gearing or fluid mechanics principles (e.g. Brzeski et al. 2017, Smith 2020, Pietrosanti et al. 2021) which enables large-scale inerter device prototypes, developed for earthquake engineering applications, to reach inertance of 10000 tons or more (e.g. Nakamura et al. 2014, Nakaminami et al. 2017). Hence, in the TMDI configuration, the inerter contributes inertia (but not weight) through large inertance by leveraging the relative kinematics (motion) during a seismic event between the secondary mass and an intermediate floor. Notably, the beneficial effect of the inerter in the TMDI configuration has been extended to the case of nonlinear energy sinks (Javidialesaadi & Wierschem 2019).

In this respect, Marian and Giaralis (2016) demonstrated numerically that the required secondary mass can be significantly reduced by trading it to inertance for fixed structural seismic performance measured in terms of top floor displacement. Further, Pietrosanti et al. (2020) and Wang & Giaralis (2021) proved that the TMDI vibration mitigation performance improves for fixed inertance as the inerter spans more floors (i.e. is connected to more than one floor below the top floor), by demonstrating analytically that the difference of the modal coordinates between the two TMDI attachment floors amplifies the inertance property. In this regard, Giaralis and Taflanidis (2018) established that the TMDI offers increased robustness to uncertainties in structural properties and seismic excitation compared to TMD, as the inertance increases, especially when the inerter connects the secondary mass two floors below the top floor. Moreover, Ruiz et al. (2018) and Taflanidis et al. (2019) showed that by judicial tuning supported by bi-objective optimal design formulations, the TMDI achieves improved structural seismic performance in terms of storey drifts and floor accelerations under stochastic ground excitations when the inerter is let to span more than one floors. Additionally, Kaveh et al. (2020) and Djerouni et al. (2022) demonstrated significantly improved seismic performance of linear buildings with TMDI spanning several floors by using large sets of non-pulse and pulse-like recorded ground motions, respectively, while Patsialis et al. (2021) extended the above conclusion to the case of inelastic (yielding) building structures.

Nevertheless, whilst TMDI configurations spanning several floors may be practically feasible in tall/landmark buildings under wind excitations by considering an internal large opening in consecutive floor slabs (see e.g. Giaralis and Petrini 2017, Dai et al. 2019), such configurations may have limited practical applicability for existing structures as well as for low-to-mid-rise buildings in high seismically active areas. Importantly, these practical limitations can be by-passed by introducing a local structural modification to the primary structure such that the difference of the modal coordinates between the floors connected by the TMDI increase, whereby exploiting the theoretical studies of Pietrosanti et al. (2020) and Wang & Giaralis (2021). To this end, Wang and Giaralis (2021) considered a TMDI configuration spanning only one (the top) floor and demonstrated that effective mitigation of wind induced oscillations in a 34-storey slender building are achieved as the top floor becomes more flexible through a local reduction of cross-sectional columns and shear walls as well as by increasing the top floor height. Still, the consideration of a soft large-height top floor may not be a practically attractive structural modification in high seismicity areas.

To this end, recognizing that a locally flexible floor can be achieved through inter-storey (or partial) seismic isolation of buildings (Villaverde 1998, Matta & De Stefano 2009, Ryan & Earl 2010, Faiella & Mele 2020), this paper investigates numerically the potential of a seismically isolated top floor equipped with a TMDI for enhanced structural seismic performance, schematically shown in Fig.1(a). In the proposed configuration termed isolated rooftop tuned mass damper inerter (IR-TMDI), the hypothesis is that the isolators yield under severe ground motion, creating a flexible rooftop which, in turn, increases the effectiveness of the TMDI for seismic energy dissipation. In this regard, the isolators of the IR-TMDI are modelled as nonlinear hysteretic elements tracing a Bouc Wen hysteretic model (Wen 1976) which is widely adopted to capture the response of elastomeric isolators (e.g. Nagarajaiah & Xiaohong 2000). From a practical viewpoint, the IR-TMDI is more advantageous than a TMDI spanning several floors as it can be readily added atop of existing building structures or included in the design of new structures as a service-only fake floor (Fig.1(a)). Indeed, the IR-TMDI resembles the rooftop isolated TMD pioneered by Villaverde (1998) (see also Villaverde and Mosqueda 1999, and Matta & De Stefano 2009), but employs a TMDI for seismic energy dissipation, rather than tuning the isolators such that the added floor plays the role of a TMD. Component-wise, the IR-TMDI is related to TMDI-equipped base isolated structures studied by De Domenico and Ricciardi (2018) and De Angelis et al. (2019), among several other researchers, in which the TMDI is housed in the basement and links the isolated layer to the ground to minimize the seismic deflection demands of the isolators. However, the IR-TMDI develops distinct dynamics compared to the systems discussed in the last publications as the inerter element is not grounded while the isolation bearings are components of the vibration absorber, rather than a part of the primary structure to be seismically protected. To this end, this paper first explores different criteria for the optimal IR-TMDI tuning by examining the primary structure response separately from the isolated rooftop deflection. Then, a comprehensive parametric study is undertaken to identify the influence of the isolated rooftop, seismic excitation, and primary structure properties to the IR-TMDI potential for seismic response mitigation. Both the optimal IR-TMDI tuning and the parametric study are facilitated by adopting a linear damped single degree of freedom (SDOF) oscillator as a proxy of the primary structure representing the dynamics of its first/dominant mode of vibration. Further, statistical linearization is employed to treat the nonlinear isolators under stationary stochastic ground excitation, thus further expediting the optimal IR-TMDI tuning and appraisal of its potential for seismic response mitigation through linear random vibrations analysis. Lastly, numerical data from nonlinear response history analyses using the recorded ground motions from the benchmark seismic vibrations control problem in Ohtori et al. (2004) are considered to verify the main trends of the seismic response of optimally tuned IR-TMDI equipped structures, focusing on the flexibility of the isolation layer. The presentation begins by describing the IR-TMDI and discussing some practical considerations before dwelling on the derivation of the nonlinear equations of motion of an IR-TMDI equipped primary structure.

2 Proposed nonlinear isolated rooftop tuned mass damper inerter (IR-TMDI) system

2.1 System description and practical considerations

Consider a generic *n*-storey planar building structure whose lateral response to horizontal seismic ground acceleration excitation, a_g, can be faithfully captured by a linear damped *n* degree-of-freedom (n-DOF) dynamical model with lumped floor masses m_k; k=1,2,…,*n* as shown in Fig. 1(a). Aiming to suppress the seismic response of the considered building (primary structure), the novel passive energy dissipation IR-TMDI system is herein considered. The system comprises an isolated slab with mass m_i placed atop of the building, as discussed by Villaverde (1998), and a linear TMDI (Marian and Giaralis 2013), placed in between the isolated slab and the topmost building slab as depicted in Fig. 1(a). With reference to the inlet in Fig.1(b), the TMDI consists of a secondary vibrating mass, m_d, which is connected to the isolated slab through a properly designed (or tuned) viscoelastic connection, modelled by a linear spring with stiffness k_d in parallel with a dashpot with damping coefficient c_d. Further, the secondary mass is linked to the topmost building slab by an inerter with inertance b (Smith 2002).

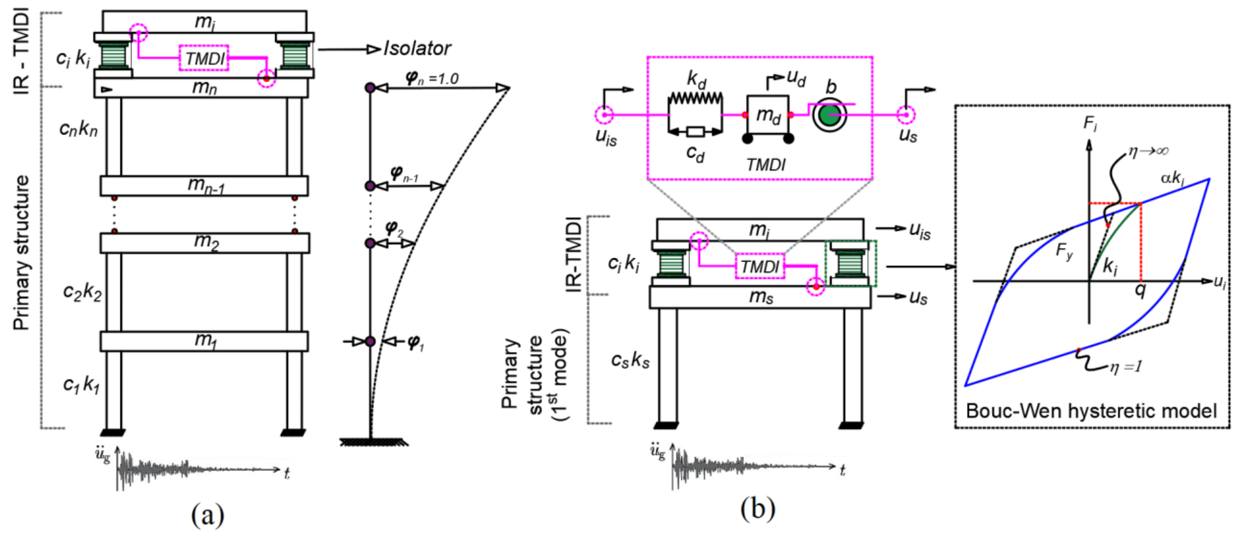

Fig. 1*: Conceptualization and mechanical modelling of the IR-TMDI system for multi-storey buildings represented by (a) lumped mass dynamic model, and (b) Simplified single-mode dynamic model*

As noted in the introduction, the proposed IR-TMDI system may be equally applicable for the seismic retrofitting of existing buildings as well as for achieving high-performing new buildings. This is because the isolated slab of the IR-TMDI can serve as a rooftop garden, as conceptualized by Matta and De Stefano (2009), or it may be part of a specially designed last floor, to house various services apart from the TMDI. In this regard, mass m_i may be taken to be comparable to the structural mass of a typical building floor, and, in every case, it should be interpreted as the top floor mass which is part of the primary/host building structure mass. Nevertheless, for the purpose of the optimal IR-TMDI design, the mass m_i needs to be treated as an integral IR-TMDI component since its value affect significantly the IR-TMDI tuning and performance as will become evident in later Sections.. Further, any standard type of bearing (isolator) for base isolated buildings (Naeim & Kelly 1999) may be used to support the IR-TMDI slab. In this work, elastomeric isolators with nonlinear hysteretic behavior are assumed, as their implementation for rooftop isolation was shown to be practically feasible through experimental work (Villaverde & Mosqueda 1999) as well as through detailed design using commercially available bearings (Villaverde 2002, Ryan & Earl 2010).

Moreover, the TMDI can be made sufficiently compact (see e.g. Pietrosanti et al 2021) and thus can be readily integrated within the isolation layer. Specifically, TMDI compactness can be facilitated by using commercial fluid viscous dampers developed for seismic applications (e.g. Berquist et al. 2019) in place of the TMDI dashpot element (see also Villaverde 2002 and Rajana et al. 2022), as well as by adopting inerter devices with large inertance and small physical mass as the one prototyped by Nakaminami et al. (2017) reaching inertance b>10000t. In this setting, the inertance b can endow exclusively the required inertia attribute to the TMDI for effective seismic response mitigation, which relaxes the need for a large secondary mass m_d. To this end, the secondary mass m_d of the IR-TMDI does not correspond to any block of steel or concrete with substantial dead weight as in conventional TMD implementations for building structures (e.g. Zemp et al. 2011, Li et al. 2011).

Instead, it is merely used to capture the influence of the relatively small self-weight (compared to the building structural weight) of the TMDI damping and inerter devices and their end connections.

As a final remark on the practicalities of the proposed IR-TMDI, note that although a TMDI may behave in a nonlinear fashion (e.g. due to the non-ideal/nonlinear inerter device behavior and/or fluid viscous damper behavior), it has been established experimentally (e.g. Gonzales-Buelga et al. 2017, Pietrosanti et al. 2021) and numerically (e.g. Brzeski & Perlikowski 2017, De Domenico et al. 2020, Rajana et al. 2022) that such nonlinear effects do not compromise the vibration mitigation potential of the TMDI configuration. If anything, such nonlinear effects are actually beneficial in earthquake engineering applications (De Domenico et al. 2020, Rajana et al. 2022). Therefore the herein adopted assumption of a linear TMDI suffices for the purpose of appraising the potential of the IR-TMDI for the structural seismic response mitigation.

2.2 Simplified single-mode structural model equipped with IR-TMDI

To support a meaningful tuning of the IR-TMDI while facilitating a comprehensive parametric investigation of the IR-TMDI seismic response performance, the simplified dynamical model in Fig. 1(b) is considered throughout this work in which the primary structure is represented by a linear damped 1-DOF modal oscillator corresponding to the fundamental mode shape vector $\boldsymbol{\varphi}$ of the *n*-DOF model. The latter is assumed to dominate the seismic response of the uncontrolled (no IR-TMDI installed) building and therefore IR-TMDI tuning is taken to target this first mode. In this context, the modal primary structure mass, m_s, inherent damping coefficient, c_s, stiffness, k_s, and seismic excitation $\ddot{x}_g$ are defined as

$$m_s = \boldsymbol{\varphi}^T \mathbf{M_s} \boldsymbol{\varphi}\,,\ c_s = \boldsymbol{\varphi}^T \mathbf{C_s} \boldsymbol{\varphi}\,,\ k_s = \boldsymbol{\varphi}^T \mathbf{K_s} \boldsymbol{\varphi}\,,\ \text{and}\ \ddot{x}_g = \frac{\boldsymbol{\varphi}^T \mathbf{M_s} \mathbf{r}}{\boldsymbol{\varphi}^T \mathbf{M_s} \boldsymbol{\varphi}} a_g\,, \tag{1}$$

respectively, where $\mathbf{M_s}$, $\mathbf{C_s}$, and $\mathbf{K_s}$, are the mass, damping, and stiffness matrices, respectively, of the *n*-DOF primary structure model, the superscript "T" denotes vector transposition and $\mathbf{r}$ is the unitary vector. By normalizing $\boldsymbol{\varphi}$ in Eq.(1) such that the modal coordinate at the *n*-th floor is equal to 1 (see Fig 1(a)), the structural modal displacement coordinate of the simplified model, u_s, relative to the ground motion coincides with the relative displacement of the *n*-th floor, expected to be the maximum across all floors for regular buildings with dominant first mode. Therefore, the modal 1-DOF oscillator with properties defined in Eq.(1) can be used as a surrogate model of the MDOF to support single-mode optimal design/tuning of inertial absorbers (Rana & Soong 1998).

Focusing on the IR-TMDI modelling, with reference to the simplified system in Fig. 2(b), the inerter is modelled as an ideal linear mechanical element developing a force given as (Smith 2002)

$$F_b = b\left(\ddot{u}_d - \ddot{u}_s\right) = b\left(\ddot{u}_i + \ddot{u}_k\right), \tag{2}$$

where $u_i = u_{is} - u_s$ and $u_k = u_d - u_{is}$ with u_d and u_{is} being the relative to the ground displacements of the TMDI secondary mass and of the isolated slab, respectively, as indicated in Fig. 1(b). In Eq.(2) and henceforth a dot over a symbol denotes time differentiation. Further, the force developing at the viscoelastic connection of the TMDI with the isolated slab is given as

$$F_v = c_d\left(\dot{u}_d - \dot{u}_{is}\right) + k_d\left(u_d - u_{is}\right) = c_d\dot{u}_k + k_d u_k \quad (3)$$

Lastly, the nonlinear restoring force of the elastomeric isolation layer is modelled as a sum of a viscoelastic and a hysteretic contribution given as

$$F_i = c_i\dot{u}_i + \alpha k_i u_i + (1-\alpha)F_y z \tag{4}$$

in which z is an auxiliary hysteretic state variable related to the isolator deflection u_i through the versatile Bouc-Wen hysteretic model expressed as (Wen 1976)

$$u_y\dot{z} = A\dot{u}_i - \gamma\left|\dot{u}_i\right|z\left|z\right|^{\eta-1} - \delta\dot{u}_i\left|z\right|^{\eta}. \tag{5}$$

Note that the Bouc-Wen model has been widely used in the scientific literature to model the behavior of laminated rubber and lead-rubber bearings (e.g. Nagarajaiah & Xiaohong 2000), as well as sliding-friction elements (Tsiatas and Karatzia 2020). Herein, a generic type of lead rubber bearing is assumed (e.g. De Domenico & Ricciardi 2018). In this context, in Eq.(4), c_i is a viscous damping coefficient modelling the energy dissipation attributed to the rubber phase of the isolation layer, k_i is the initial stiffness prior to the yielding of the lead cores, αk_i is the post-yielding stiffness, and F_y is the yielding strength of the isolators (see also Fig.1(b)). Further, in Eq.(5), u_y is the yielding displacement, while δ, γ, η and A are the Bouc-Wen model parameters which control the shape and inclination of the hysteretic F_i - u_i loop (Wen 1976, Ikhouane et al 2006). In the numerical part of this work, the Bouc-Wen parameters are taken as $\delta = \gamma = 0.5$, $A = \eta = 1$ and $\alpha = 0.10$, which model a standard smooth hysteretic behaviour, as shown in the inlet of Fig.1(b), widely adopted in the literature to model lead rubber isolators (e.g. De Domenico & Ricciardi 2018).

Moreover, the stiffness of the isolated rooftop is quantified by the post-yielding effective period of the isolation layer given as (Jangid 2010)

$$T_i = 2\pi\sqrt{\frac{m_i}{\alpha k_i}} = 2\pi\sqrt{\left(\frac{u_y}{F_0\, g\, \alpha}\right)} \tag{6}$$

where g = 9.81m/s^2 and F_o is the normalized yielding strength defined as

$$F_o = \frac{F_y}{m_i g}. \tag{7}$$

2.3 Nonlinear equations of motion of the simplified model

Using the modelling assumptions discussed above, the equations of motion of the simplified model in Fig.1(b) are written as

$$\begin{aligned} &m_s\ddot{u}_s + c_s\dot{u}_s + k_s u_s - F_i - F_b = -m_s\ddot{x}_g \\ &m_i\left(\ddot{u}_i + \ddot{u}_s\right) + F_i - F_v = -m_i\ddot{x}_g \\ &m_d\left(\ddot{u}_k + \ddot{u}_i + \ddot{u}_s\right) + F_v + F_b = -m_d\ddot{x}_g \end{aligned} \tag{8}$$

By introducing the dimensionless parameters: natural frequency of the primary structure, ω_s, and of the TMDI, ω_d, defined as

$$\omega_s = \sqrt{\frac{k_s}{m_s}} \text{ and } \omega_d = \sqrt{\frac{k_d}{b+m_d}} , \tag{9}$$

critical damping ratio of the primary structure, ξ_s, of the isolation layer, ξ_i, and of the TMDI, ξ_d, defined as

$$\xi_s = \frac{c_s}{2m_s\omega_s} \;,\; \xi_i = \frac{c_i}{2\omega_i m_i} \text{ and } \xi_d = \frac{c_d}{2(m_d+b)\omega_d} , \tag{10}$$

mass ratios of the isolated slab, μ_i, and of the TMDI, μ_d, and inertance ratio, β, defined as

$$\mu_i = \frac{m_i}{m_s} \;,\; \mu_d = \frac{m_d}{m_s} \text{ and } \beta = \frac{b}{m_s} , \tag{11}$$

the equations of motion in Eq.(8) are further written in matrix form as

$$\mathbf{M\ddot{u}} + \mathbf{C\dot{u}} + \mathbf{Ku} + \mathbf{p}z = -\mathbf{d}\ddot{x}_g , \tag{12}$$

where

$$\mathbf{M} = \begin{bmatrix} 1 & -\beta & -\beta \\ \mu_i & \mu_i & 0 \\ \mu_d & \mu_d+\beta & \mu_d+\beta \end{bmatrix} \;,\; \mathbf{C} = \begin{bmatrix} 2\xi_s\omega_s & -2\xi_i\omega_i & 0 \\ 0 & 2\xi_i\omega_i & -2\xi_d\omega_d(\mu_d+\beta) \\ 0 & 0 & 2\xi_d\omega_d(\mu_d+\beta) \end{bmatrix} ,$$
$$\mathbf{K} = \begin{bmatrix} \omega_s^2 & -\alpha\mu_i\omega_i^2 & 0 \\ 0 & \alpha\mu_i\omega_i^2 & -\omega_d^2(\mu_d+\beta) \\ 0 & 0 & \omega_d^2(\mu_d+\beta) \end{bmatrix} \;,\; \mathbf{p} = \begin{bmatrix} -\mu_i(1-\alpha)F_o g \\ \mu_i(1-\alpha)F_o g \\ 0 \end{bmatrix} \;,\; \mathbf{d} = \begin{bmatrix} 1 \\ \mu_i \\ \mu_d \end{bmatrix} \text{ and } \mathbf{u} = \begin{bmatrix} u_s \\ u_i \\ u_k \end{bmatrix}. \tag{13}$$

It is important to recognize that the system of equations in Eq.(12) is nonlinear due to the nonlinear (hysteretic) relationship between the coordinates z and u_i in Eq.(5). This nonlinearity significantly impedes the analysis and, therefore, the optimal design (or tuning) of IR-TMDI by requiring computationally expensive nonlinear response history analyses. To this end, Eq.(5) is treated via stochastic linearization in the next section to derive an equivalent linear system with the view of expediting the IR-TMDI tuning and seismic response assessment under stochastic seismic excitation.

3 Stochastic Linearization and random vibration analysis

3.1 Equivalent linear system

Commonly, stochastic ground excitation models are used in the optimal tuning of inertial dampers to account for the uncertain nature of the earthquake ground motion (e.g. Marian and Giaralis 2014, Taflanidis et al. 2019). For linear structural systems and absorbers, this is significantly facilitated by straightforward application of linear random vibration analysis. In the presence of nonlinearities, computationally efficient stochastic linearization (SL) approaches can be employed for the task (e.g. Sgobba and Marano 2010, Mitseas et al. 2018) which approximate the nonlinear stochastic seismic response of structures by the response of an underlying equivalent linear dynamic system (ELS) under the same stochastic ground excitation without the need for nonlinear response history analysis (Spanos & Giaralis 2013). To this end, the SL approach introduced by Wen (1980) for the Bouc Wen model is herein applied to substitute Eq. (5) with an equivalent linear equation given as

$$u_y \dot{y} + c_{eq}\dot{x}_i + k_{eq} y = 0\,. \tag{14}$$

In the last expression, y and $\dot{x}_i$ are response processes of the ELS corresponding to the ordinates z and u_i of the nonlinear system. Further, c_{eq} and k_{eq} are deterministic parameters obtained by minimising the mean square error between the nonlinear system defined by Eqs.(5) and (12) and the ELS (Eqs.(14) and (12)), under the same $\ddot{x}_g$ stationary Gaussian stochastic excitation process. Using the fact that y and $\dot{x}_i$ are jointly Gaussian, the equivalent linear parameters in Eq.(14) are given as (Wen 1980)

$$c_{eq} = \sqrt{\frac{2}{\pi}}\left(\gamma \frac{E[\dot{x}_i y]}{\sigma_{\dot{x}_i}} + \delta\sigma_y\right) - A \quad \text{and} \quad k_{eq} = \sqrt{\frac{2}{\pi}}\left(\gamma\,\sigma_{\dot{x}_i} + \delta\frac{E[\dot{x}_i y]}{\sigma_y}\right), \tag{15}$$

for η = 1, where E [.] is the mathematical expectation operator and σ_x denotes the standard deviation of the process x. Importantly, the equivalent linear parameters c_{eq} and k_{eq} are unknown as they depend on the unknown response statistics $\sigma_{\dot{x}_i}$ and σ_y of the ELS. Therefore, iterative linear random vibration analyses is required to determine the parameters in Eq.(15) together with the response statistics of the ELS. Such analyses can be efficiently undertaken for different seismic stochastic excitations in state space as discussed in the following section.

3.2 Random vibration analysis and determination of the equivalent linear parameters

In this work, efficient linear random vibration analysis is performed in state-space to obtain response statistics of the ELS, together with the equivalent linear parameters in Eq.(15) in the context of stochastic linearization, under different stationary stochastic excitations. This is achieved by first expressing the equations of motion of the ELS in state-space as

$$\dot{\mathbf{x}} = \mathbf{A}\mathbf{x} + \mathbf{B}w \tag{16}$$

where **A** is the state matrix, **B** is the excitation vector, **x** is the vector of the unknown state variables, and w is Gaussian white noise excitation. Then, the covariance matrix $\mathbf{\Gamma}$ collecting all second-order response statistics of the processes in vector **x** can be determined by solving the Lyapunov equation

$$\mathbf{A\Gamma} + \mathbf{\Gamma A}^{\mathbf{T}} + 2\pi S_o \mathbf{B}\mathbf{B}^T = 0 \tag{17}$$

where S_o is the spectral intensity of the white noise w. In the computational part of this study, the built-in MATLAB function *lyap* is used to obtain numerically the covariance matrix $\mathbf{\Gamma}$. The diagonal elements of the latter matrix are the variances of the states in vector $\mathbf{x}$ while the off-diagonal elements are the cross-variances of all the states.

Notably, Eqs. (15) and (16) can be used to determine the response statistics of the ELS, for given equivalent linear parameters in Eq.(14), under stationary white noise as well as colored noise (filtered Kanai-Tajimi) excitations. For stationary white noise excitation, the state matrix, excitation vector, and state variable vector are written as

$$\mathbf{A} = \begin{bmatrix} 0_{(3,3)} & \mathbf{I}_{(3)} & \mathbf{0}_{(3,1)} \\ -\mathbf{M}^{-1}\mathbf{K} & -\mathbf{M}^{-1}\mathbf{C} & -\mathbf{M}^{-1}\mathbf{P} \\ \mathbf{0}_{(1,3)} & \begin{Bmatrix} 0 & -\dfrac{c_{eq}}{q} & 0 \end{Bmatrix} & -\dfrac{k_{eq}}{q} \end{bmatrix}, \quad \mathbf{B} = \begin{Bmatrix} \mathbf{0}_{(3,1)} \\ -\mathbf{M}^{-1}\mathbf{d} \\ 0 \end{Bmatrix}, \quad \mathbf{x} = \begin{Bmatrix} x_s \\ x_i \\ x_k \\ \dot{x}_s \\ \dot{x}_i \\ \dot{x}_k \\ y \end{Bmatrix}, \tag{18}$$

respectively, where the response coordinates of the ELS are denoted by a different symbol from those of the nonlinear system in Eqs. (5) and (12) (i.e. x is used in place of u, and y in place of z as discussed before) to emphasize that the ELS response is different (i.e. an approximation) of the response of the nonlinear system. In Eq.(18), $\mathbf{0}_{(m,n)}$ is the m-by-n zero matrix, $\mathbf{I}_{(m)}$ is the m-by-m identity matrix, and the exponent "-1" demotes matrix inversion. Further, the spectral intensity S_o in Eq. (17) is related to the peak ground acceleration (PGA) for the case of clipped white noise excitation with double-sided power spectral density function using the expression

$$S_{\mathbf{o}} = \frac{\mathrm{PGA}^2}{18\omega_{\mathrm{c}}} \tag{19}$$

where ω_c is the cut-off frequency of the excitation, derived under the approximate "3σ" rule.

In case it is deemed important to account for site soil conditions, the ground excitation can be modelled by a Gaussian stationary colored noise, represented in the domain of frequencies ω by the widely-used for the purpose filtered Kanai-Tajimi (K-T) spectrum given as (Clough and Penzien 2003)

$$S(\omega) = S_o \frac{\omega_g^4 + 4\xi_g^2\omega_g^2\omega^2}{\left(\omega_g^2 - \omega^2\right)^2 + 4\xi_g^2\omega_g^2\omega^2} \frac{\omega^4}{\left(\omega_f^2 - \omega^2\right)^2 + 4\xi_f^2\omega_f^2\omega^2}, \tag{20}$$

where ω_g and ξ_g are the natural frequency and damping ratio of the soil, respectively, which is modelled as a white noise excited linear 1-DOF system with spectral intensity S_o. Morevoer, ω_f and ξ_f are parameters of a high-pass filter incorporated in Eq.(20) to eliminate spurious low-frequency content. In subsequent sections, different soil conditions are accounted for by using the parameters in Table 1 derived in Giaralis and Spanos (2012).

Table 1: Filtered Kanai-Tajimi parameters for different soil conditions (Giaralis and Spanos 2012)

Soil type	ω_g (rad/s)	ξ_g	ω_f (rad/s)	ξ_f	Dominant period $2\pi/\omega_g$ (s)
firm	10.73	0.78	2.33	0.90	0.59
soft	5.34	0.88	2.12	1.17	1.18

Conveniently, the spectrum in Eq.(20) can be readily incorporated in the state-space formulation in Eq.(16) as a pre-filter excited by white noise (e.g. Taflanidis and Giaralis 2018) by augmenting the expressions in Eq.(18) as follows

$$\mathbf{A}=\begin{bmatrix} 0_{(3,3)} & \mathbf{I}_{(3)} & \mathbf{0}_{(3,1)} & \mathbf{0}_{(3,1)} & \mathbf{0}_{(3,1)} & \mathbf{0}_{(3,1)} & \mathbf{0}_{(3,1)} \\ -\mathbf{M}^{-1}\mathbf{K} & -\mathbf{M}^{-1}\mathbf{C} & -\mathbf{M}^{-1}\mathbf{p} & \omega_f^2\mathbf{M}^{-1}\mathbf{d} & -\omega_g^2\mathbf{M}^{-1}\mathbf{d} & 2\xi_f\omega_f\mathbf{M}^{-1}\mathbf{d} & -2\xi_g\omega_g\mathbf{M}^{-1}\mathbf{d} \\ \mathbf{0}_{(1,3)} & \left\{0 \quad -\dfrac{c_{eq}}{q} \quad 0\right\} & -\dfrac{k_{eq}}{q} & 0 & 0 & 0 & 0 \\ \mathbf{0}_{(1,3)} & \mathbf{0}_{(1,3)} & 0 & 0 & 0 & 1 & 0 \\ \mathbf{0}_{(1,3)} & \mathbf{0}_{(1,3)} & 0 & 0 & 0 & 0 & 1 \\ \mathbf{0}_{(1,3)} & \mathbf{0}_{(1,3)} & 0 & -\omega_f^2 & \omega_g^2 & -2\xi_f\omega_f & 2\xi_g\omega_g \\ \mathbf{0}_{(1,3)} & \mathbf{0}_{(1,3)} & 0 & 0 & -\omega_g^2 & 0 & -2\xi_g\omega_g \end{bmatrix},$$

$$\mathbf{B}=\{0 \quad 0 \quad 0 \quad 0 \quad 0 \quad 0 \quad 0 \quad 0 \quad 0 \quad 0 \quad -1\}^T, \tag{21}$$

$$\mathbf{x}=\{x_s \quad x_i \quad x_k \quad \dot{x}_s \quad \dot{x}_i \quad \dot{x}_k \quad y \quad x_f \quad x_g \quad \dot{x}_f \quad \dot{x}_g\}^T$$

Thus, Eq.(17) can be used in conjunction with Eq.(21) to determine all the response statistics of the ELS for filtered Kanai-Tajimi excitation. In this case, the spectral intensity S_o is related to the PGA by (Sgobba and Marano 2010)

$$S_o=\left(\frac{4}{9\pi}\right)\frac{\xi_g \mathrm{PGA}^2}{\omega_g\sqrt{1+4\xi_g^2}}. \tag{22}$$

As previously discussed, the response statistics of the ELS in matrix $\boldsymbol{\Gamma}$ need to be determined together with the ELS parameters c_{eq} and k_{eq} by using iteratively Eqs. (15) and (17) until convergence (Roberts & Spanos 2003). For numerical implementation, seed values c_{eq} = -1 and k_{eq} = 0 are assumed in the computational part of this work and iterations are performed until consecutive values of both of the ELS parameters differ by less than 10^{-6} (stoppage criterion).

4 Optimal IR-TMDI tuning

4.1 Optimal design problem formulation and alternative tuning criteria (objective functions)

In this section, optimal tuning of the IR-TMDI in Fig.1 is sought by considering the response of the ELS defined in Section 3 with primary structure properties ω_s and ξ_s under stationary stochastic seismic excitation. For this purpose, an optimal IR-TMDI design problem is formulated involving 7 independent design parameters.

These are the TMDI damping and frequency ratios, ξ_d and $\lambda = \omega_d/\omega_s$, collected in vector $\boldsymbol{\upsilon}$ and treated as primary design variables, as well as the isolation layer damping and effective natural period, ξ_i and T_i, and the IR-TMDI inertial ratios μ_i, μ_d, and β collected in vector $\mathbf{v}$ and treated as secondary design variables. In this context, the proposed optimal IR-TMDI design/tuning problem seeks to determine the primary parameters in $\boldsymbol{\upsilon}$, within a prespecified search range [$\boldsymbol{\upsilon}_{\min}$, $\boldsymbol{\upsilon}_{\max}$], to minimize an objective function J (tuning criterion), dependent on the ELS stationary response statistics, for a set of fixed secondary parameters in $\mathbf{v}$. This distinction between primary and secondary IR-TMDI design parameters is purposely made to facilitate comprehensive parametric investigations, presented in a subsequent section, aiming to quantify the influence of different IR-TMDI properties to the seismic response mitigation and performance of IR-TMDI for various primary structure properties and stochastic seismic excitations. Mathematically, the considered optimal IR-TMDI tuning problem can be written as

$$\min_{\boldsymbol{\upsilon}}\left\{J\left(\boldsymbol{\upsilon}|\mathrm{v}\right)\right\} \quad \text{with} \quad \boldsymbol{\upsilon}_{min} \le \boldsymbol{\upsilon} \le \boldsymbol{\upsilon}_{max} \quad \text{where} \quad \boldsymbol{\upsilon} = \left\{\xi_d, \lambda = \frac{\omega_d}{\omega_s}\right\} \quad , \quad \mathrm{v} = \left\{\xi_i, T_i, \mu_i, \mu_d, \beta\right\} \tag{23}$$

The optimal tuning problem in Eq.(23) can accommodate different tuning criteria, targeting the minimization of specific response quantities based on the choice of the objective function J. In this respect, one viable tuning criterion is the maximization of the TMDI energy dissipation index (EDI), proposed by Pietrosanti et al. (2017). This tuning criterion was shown to achieve efficient optimal TMDI designs for the seismic response mitigation of base isolated structures, striking a good balance between reducing seismic displacement and acceleration demands (De Domenico & Ricciardi 2018, De Angelis et al. 2019). In this work, the EDI is defined as the portion of the input stationary stochastic seismic energy dissipated by the TMDI damping element with coefficient c_d over the total energy dissipated by the ELS. The latter is the sum of the energy dissipated by the primary structure (through the inherent damping coefficient c_s), the TMDI, and the isolators (through the viscous damping coefficient c_i and the hysteretic behavior), as detailed in the energy balance analysis undertaken in the Appendix A. The EDI is computed as (see Appendix A for derivation)

$$0 \le \mathrm{EDI} = \frac{c_d \sigma^2_{\dot{x}_k}}{c_s \sigma^2_{\dot{x}_s} + c_d \sigma^2_{\dot{x}_k} + c_i \sigma^2_{\dot{x}_i} + \left(1-\alpha\right) F_y E\left[\dot{x}_i y\right]} \le 1 \tag{24}$$

and the associated objective function supporting a minimization problem in Eq.(23) is expressed as (De Domenico & Ricciardi 2018)

$$J_1 = \mathrm{FEI} = 1 - \mathrm{EDI}\ , \tag{25}$$

where FEI stands for the filtered energy index. Notably, FEI signifies the portion of the total energy that is not dissipated by the TMDI. Thus, the minimization of FEI leads to IR-TMDI designs which maximize energy dissipation to take place by the TMDI rather than by the isolation layer for given isolation layer properties and IR-TMDI inertial (mass and inertance) properties.

Further to the FEI, two alternative tuning criteria are also considered since they have been widely used in the optimal TMDI tuning of non-isolated structures under stochastic seismic excitations (e.g. Marian and Giaralis

2014, Pietrosanti et al. 2017, Rajana et al. 2022). One criterion seeks to minimize the relative displacement (deflection) variance of the primary structure and is introduced in Eq.(23) by the normalized objective function

$$J_2 = \frac{\sigma_{x_s}^2}{\sigma_{x_o}^2}, \tag{26}$$

where x_o is the relative displacement of the uncontrolled primary structure (i.e. without IR-TMDI). This criterion is well-related to the minimization of the structural damage in the primary structure. The other criterion seeks to minimize the total acceleration variance of the primary structure and is introduced in Eq.(23) by the normalized objective function

$$J_3 = \frac{\sigma_{\ddot{x}_{s,abs}}^2}{\sigma_{\ddot{x}_{o,abs}}^2} \tag{27}$$

where $x_{s,abs}$ and $x_{o,abs}$ are the total acceleration of the controlled and the uncontrolled primary structure for the same stochastic excitation. The latter criterion is well-related to the minimization of the damage of non-structural components and equipment housed in the primary structure.

For all the adopted objective functions in Eqs.(25-27), the optimization problem in Eq.(23) is numerically solved using standard pattern search (Charles and Dennis, 2008) implemented in the built-in MATLAB® command `fminsearch`. In all the subsequent numerical work, the boundaries of the search range is set as $\boldsymbol{\upsilon}_{\min}$= {0,0} and $\boldsymbol{\upsilon}_{\max}$= {2,2}. This search range suffices to determine a global optimum of the problem in Eq.(23) which was found to be convex for all sets of IR-TMDI parameters, primary structure properties, objective functions, and stochastic excitations investigated in the following Sections.

4.2 Numerical investigation of alternative tuning criteria

A numerical investigation is herein undertaken to appraise the potential of the three previously discussed tuning criteria for yielding advantageous IR-TMDI designs. This is pursued by solving the optimization problem in Eq.(23) for the objective functions in Eqs.(25)-(27) for different inertance ratios varying within the range [0, 25%] and for white noise excited ELS with structural period $T_s = 2\pi/\omega_s$= 1s, structural inherent damping ratio ξ_s *=5%*, isolation mass ratio μ_i *= 10%*, isolation period T_i*=3.5s* (assuming yielding displacement u_y=2cm and normalized yielding strength F_o= 0.065 in Eq.(7)), isolation damping ratio ξ_i=5%, and secondary mass ratio μ_d = 0.5%. The white noise intensity is assumed to correspond to PGA=0.3g with cut-off frequency $\omega_c = 15\pi$ in Eq.(19). Numerical results obtained from the optimal tuning and from the ELS response with optimal IR-TMDIs are presented in Fig. 2. Specifically, 9 different quantities are examined, described in the titles of each of the 9 panels of Fig.2, against the inertance ratio for each of the three different tuning criteria. The top row of panels pertain to results from optimal tuning: the FEI objective function in Eq.(25) is plotted in Fig.2(a), while the optimal values of IR-TMDI primary design parameters in vector $\boldsymbol{\upsilon}$ of Eq.(23) are plotted in Figs.2(b) and 2(c). The middle row of panels in Fig.2 present ELS response variance data from optimally tuned IR-TDMI normalized by response variances of the uncontrolled primary structure (with no IR-TMDI): Fig.2(d) plots the normalized relative displacement variance of the primary structure J_2 in Eq.(26), Fig.2(e) plots the deflection variance of the isolated layer normalized as in the J_2 index, and Fig.2(f) plots the normalized absolute acceleration variance of the primary structure J_3 in Eq.(27). Lastly, the bottom row of panels in Fig.2 present data from forces developing in the ELS with optimally tuned IR-TMDI: Fig.2(g) plots the variance of the inerter force in Eq.(2) using ELS response acceleration variances normalized by the variance of the inertia force developed in the uncontrolled structure, Fig.2(i) plots the variance of the isolators' force in Eq.(4) using ELS response statistics normalized by the variance of the inherent damping force developed in the uncontrolled structure, and Fig.2(h) plots the variance of the force developed at the TMDI damping element (e.g. $F_d = c_d \sigma^2_{\dot{x}_k}$) using the same normalization as in Fig.2(i).

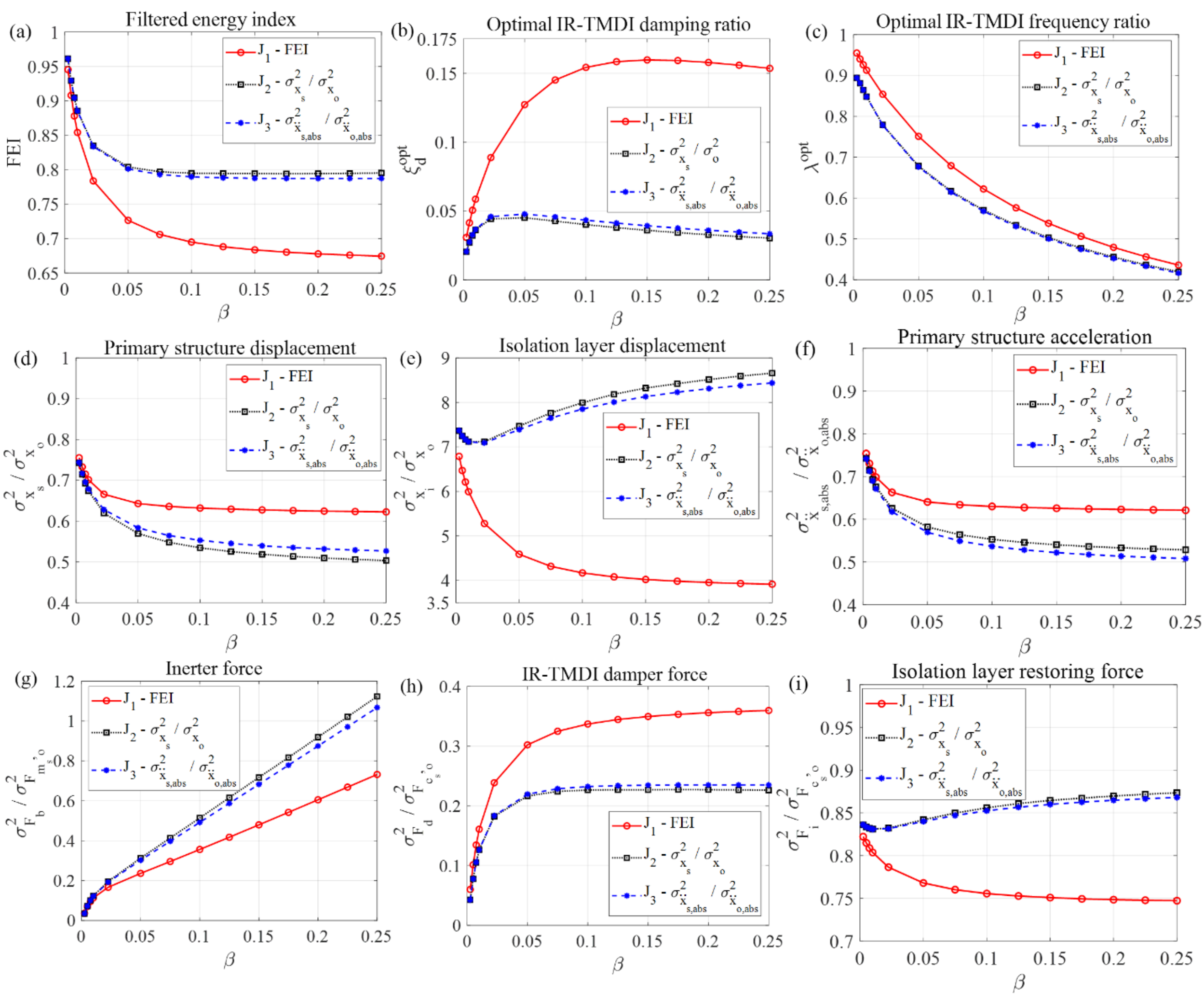

Fig. 2: *Optimal IR-TMDI properties and normalized system response variances plotted against the inertance ratio for different tuning criteria (objective functions) and for T_s=1s, ξ_s=5%, μ_i=10%, T_i=3.5s, ξ_i=5%, μ_d=0.5%, white noise excitation with PGA=0.3g and ω_c=15π* (Base case).

It is important to note that the ordinates of the plots in the middle and the bottom row of the panels are herein used solely to establish relative seismic response trends and, thus, are interpreted in a relative rather than in an absolute sense. This is because they correspond to linear systems (ELSs) under stationary base excitation which have limited capability for dependable prediction of the expected seismic response of IR-TMDI structures. This is due to the fact that actual seismic excitation is non-stationary, as reflected on the time-evolving amplitude and frequency content of recorded earthquake strong ground motions (e.g. Spanos et al. 2007), while the potential of the ELS to estimate the nonlinear behaviour of the hysteretic isolators is restricted by the well-known limitations of statistical linearization (e.g. Roberts & Spanos 2003, Spanos & Giaralis 2013).

From the top row of panels in Fig.2, it is seen that IR-TMDI optimal tuning based on the FEI criterion achieves significantly higher TMDI energy dissipation for any given value of inertance ratio compared to tunings aiming at structural displacement minimization, J_2, or acceleration minimization, J_3, as readily deduced from Fig.2(a). This is due to a significantly higher optimal TMDI damping ratio obtained by the FEI-based tuning compared to the other two tuning criteria as seen in Fig.2(b), (e.g. more than three times higher for β>7%). Notably, differences in the optimal TMDI frequency ratio among the three tuning criteria are non-negligible as seen in Fig.2(c), but are much less prominent compared to differences in the optimal TMDI damping ratio. Still, the system response kinematics data shown in the middle row of panels in Fig.2, evidence that FEI-based tuning results in lower primary response reductions in terms of displacement variance, Fig. 2(d), and acceleration variance, Fig. 2(f), compared to the other two examined tuning criteria, for any given inertance ratio. Further, it is seen in Figs.2(d) and 2(f) that, as expected, J_2-based tuning achieves the best (i.e. lowest) structural displacement performance across the competing tuning criteria while J_3-based tuning achieves the best structural acceleration performance, respectively.

Nevertheless, FEI-based tuning poses significantly lower deflection demands to the isolation layer (i.e. to the LRB bearings) compared to the tunings using J_2 and J_3 criteria as shown in Fig.2(e). For example, the required isolation layer deflection variances for both J_2- and J_3-based tuning, for $\beta \geq 10\%$, are more than twice that of FEI-based tuning. Furthermore, for FEI-based tuning, isolation deflection demands decrease with inertance, while other competing tuning criteria necessitate higher isolation layer deflection with increasing inertance. At the same time, FEI-based tuning reduces significantly the forces exerted by the IR-TMDI to the primary structure compared to the J_2 and J_3 based tunings, that is the inerter force and the isolators' force as evidenced in Figs.2(g) and 2(i), respectively. Further, the reduction of these forces become increasingly higher as the inertance ratio increases. Specifically, it is seen in Fig.2(g) that for any given inertance value, the FEI-based normalized inerter force variance is much lower compared to the values pertaining to the other tunings. More importantly, the reduction of the inerter forces increases monotonically with the inertance ratio as the rates of increase of the inerter force variance with inertance (slope of the curves in Fig.2(g)) is appreciably lower for the FEI-based tuning compared to the J_2 and J_3 based tunings. Additionally, as with the inerter force variance, it is observed from Fig.2(i) that the variance of the isolators' forces for FEI-based tuning vis-à-vis J_2 and J_3 based tuning is always lower while the benefit (difference) increases with inertance. This is because the isolators' force reduces appreciably with inertance for FEI-based tuning, while it slightly increases with inertance for the alternative tunings. In this regard, although FEI-based tuning results in lower displacement and acceleration reductions compared to the J_2 and J_3 based tunings, it is overall more advantageous from a practical viewpoint since it yields reduced requirements for isolation layer deflection and for isolators' and inerter force transmission which, collectively, become more significant as the inertance increases. Notably, similar trends are found for different values of T_i and T_s than those assumed in Fig.2, though results are not herein reported for the sake of brevity. To this end, it is recommended that IR-TMDI is tuned for TMDI energy dissipation maximization (i.e. FEI tuning criterion in Eq.(25)) which echoes previous recommendations in the literature on optimal tuning of TMDI with grounded inerter for the seismic protection of base isolated structures (De Domenico & Ricciardi 2018, De Angelis et al. 2019).

As a closing remark to this section, it is worth noting that the recommended FEI-based tuning results in higher TMDI damping forces compared to J_2 and J_3 based tunings as seen in Fig.2(h). The higher values in the TMDI damping force variance are a direct result of the higher optimal TMDI damping coefficients coming from the FEI-based tuning in Fig.2(b) for any arbitrary inertance ratio. In this respect, it is concluded that the FEI-based tuning supports an IR-TMDI design whereby the TMDI is the main actor in mitigating primary structure seismic response, as opposed to the bearings of the seismic isolation layer. In this setting, the significance of the TMDI over the isolators for the seismic response mitigation increases as the inertance property increases. Indeed, for FEI-based tuning, TMDI damping and inerter forces increase with inertance (Figs.2(g) and 2(h), respectively) while the isolators' deflection and force demands reduce with inertance (Figs.2(e) and 2(i), respectively). The latter consideration is of paramount practical importance since inertance can readily and economically scale-up in real-life inerter devices (e.g. Nakamura et al. 2014, Nakaminami 2017, Pietrosanti et al. 2021), thus yielding an increasingly efficient IR-TMDI for the seismic protection of primary building structures.

5 Parametric investigation and assessment of optimally tuned IR-TMDI

Having established a practically meritorious optimal tuning criterion for the proposed IR-TMDI (i.e. FEI in Eq.(25)), this section presents and discusses numerical data from a comprehensive parametric investigation aiming to assess the influence of the IR-TMDI properties (i.e. secondary design parameters in vector **v** in Eq.(23)), of the primary structure properties, and of the stationary excitation properties to the effectiveness of FEI-based optimally tuned IR-TMDI. In doing so, the system properties and excitation considered in producing the results of Fig.2 are taken as the base case whereas one parameter/property is let to vary each time to examine its influence/importance. With one exception which will be pointed out later in the text, all numerical results in this section are presented using the same plotting pattern and normalizations as in Fig.2 to facilitate comparisons across the different cases and parameters considered vis-à-vis the base case. As a previously highlighted word of caution, the magnitude of the reported kinematics (deflections) and forces in this section have only a relative significance and are herein used to establish relative trends of the seismic response under varying system and excitation properties. This is because they are derived from ELSs under stationary base excitation with limited capability for estimating the expected seismic response of nonlinear IR-TMDI equipped structures. The presentation begins by examining the influence of the isolation layer properties as they deviate from the base case in Fig.2.

5.1 Influence of the isolated rooftop properties

The stiffness k_i of the isolation bearings is expected to influence significantly the IR-TMDI seismic response reduction potential, as it directly relates to the deflection of the isolated rooftop under seismic excitation and, therefore, to the level of engagement of the TMDI. To quantify this influence, Fig.3 plots numerical data for 5 different values of the effective natural period of the isolation layer T_i in Eq.(6) obtained by varying the stiffness k_i of the bearings, while all other system and excitation parameters are the same as in the base case of Fig.2. It is found that the consideration of more flexible isolators or, equivalently, of longer period T_i, facilitates the seismic energy dissipation by the TMDI as manifested by the reduced values of FEI with T_i for any given inertance ratio in Fig.3(a). This effect results in improved primary structure performance as demonstrated by reductions to both the structural displacement and acceleration variances in Figs.3(d) and (f), respectively, as the period T_i elongates for any value of inertance ratio with β>2.5%. These improvements become more significant as the inertance ratio increases and are due to larger inerter and damper forces developed by the TMDI with increasing T_i as shown in Figs.3(g) and 3(h). It is worth noting that these higher TMDI forces are generated by the increased relative accelerations and velocities through the inerter and the damping elements. This is readily deduced for the inerter force in Fig.3(g) since the inerter force variance increases with T_i for any fixed inertance. Further, in Fig.3(h), the damping force variance increases with T_i for any given value of inertance, even though the optimal damping coefficient in Fig.3(b) reduces with T_i for the same inertance. Clearly, this is only possible if the relative velocity across the TMDI damping element increases with T_i.

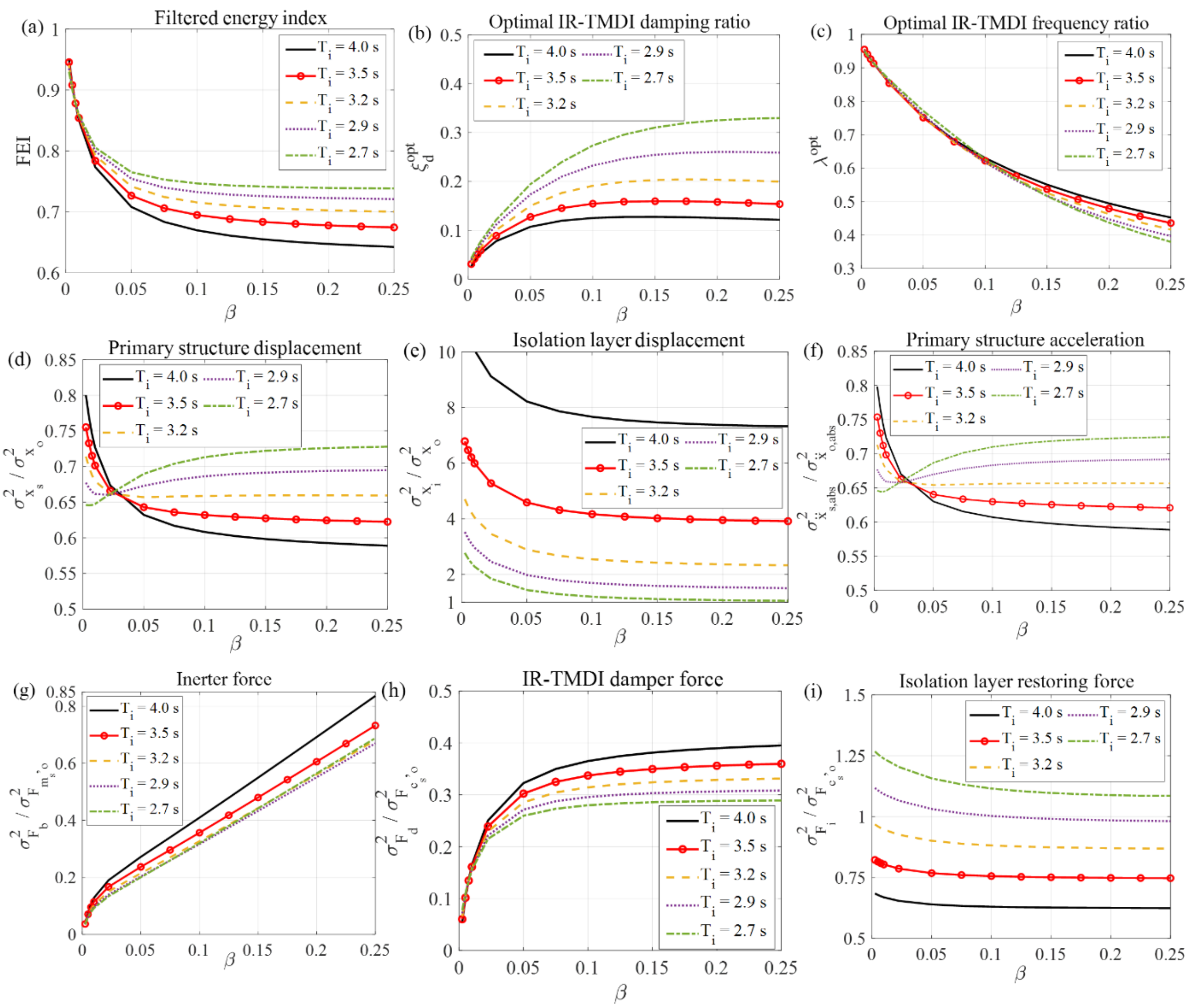

Fig. 3*: Optimal IR-TMDI properties using the FEI tuning criterion and normalized system response variances plotted against the inertance ratio for different isolation layer periods T_i and for T_s=1s, ξ_s=5%, μ_i=10%, ξ_i=5%, μ_d=0.5%, white noise excitation with PGA=0.3g and ω_c=15π.*

Nevertheless, the improved primary structure performance with T_i comes at the cost of increased deflections in the isolation layer as seen in Fig.3(e). In this regard, there is a trade-off between primary structure response and isolated layer response which is regulated by the stiffness of the isolation layer. At the same time, although improved primary structure performance is always achieved by the IR-TMDI compared to the uncontrolled structure (i.e. ordinates in Figs.3(d) and 3(f) are well below 1), the primary structure performance deteriorates as inertance increases when relatively stiff isolators are adopted (see cases of T_i=2.7s and 2.9s in Figs. 3(d) and 3(f)). To this end, a judicial selection of the isolators' stiffness k_i is required to promote higher values of T_i in conjunction with high inertance, depending on the desired level of primary structure seismic response mitigation, while ensuring the isolators' ability to perform large deflections without facing stability issues (see also Ryon & Earl 2010). This recommendation is further supported by the fact that the force demands of the isolators reduce as T_i elongates for any inertance value as seen in Fig.3(i). Importantly, the latter observation confirms that the FEI-based tuned IR-TMDI improves the primary structure performance through a better engagement of the TMDI manifested by higher TMDI inerter and damping forces as the isolators become more flexible, provided there is sufficient inertance (e.g. β>2.5% for the system considered), rather than through the action of the isolators (i.e. through the force transmitted by the isolators to the primary structure).

Next, the influence of the isolated rooftop mass m_i is examined by plotting in Fig.4 the same type of numerical data as in previous figures for 4 different values of the mass ratio μ_i including the value of the base case, μ_i= 10%, while all other ELS and excitation parameters are the same as in the base case. To this effect, a different isolators' stiffness k_i is chosen for each μ_i value such that the isolation layer period T_i is kept constant and equal to the base case (i.e. T_i= 3.5s). This consideration establishes a meaningful comparison across systems with different mass ratios μ_i and is widely employed in the literature to compare inter-storey isolated buildings with different ratios of masses above and below the isolated layer (e.g. Faiella & Mele 2019). Parenthetically, it is worth pointing out that if only μ_i is let to vary, then the isolation layer period T_i in Eq.(6) will change accordingly, resulting in similar response trends as those in Fig.3.

It is seen in Fig.4(a) that the increase of the rooftop mass with constant T_i results in reductions to the FEI index upon optimal IR-TMDI tuning (i.e. more energy is dissipated by the TMDI) for any given value of inertance. These reductions in FEI yield improved primary structure performance for both displacement and accelerations as shown in Figs.4(d) and 4(f), respectively. Here, the improved structural performance is due to significant increase of the force exerted to the primary structure by the isolators with μ_i, as seen in Fig.4(i), while the kinematics of the isolated rooftop reduce with μ_i, as evidenced by the reduced isolation layer deflections in Fig.4(e). As a result, the level of engagement of the inerter (i.e. the relative acceleration between the TMDI secondary mass and the top floor of the primary structure) reduces with μ_i, resulting in lower inerter force exerted to the primary structure in Fig.4(g) as μ_i increases for fixed inertance. Still, the TMDI damping force increases with μ_i due to the higher optimal damping ratios in Fig.4(b).

In this regard, it is found that the IR-TMDI achieves improved seismic primary structure performance either by increasing the isolation rooftop period/flexibility, T_i, (for the same additive rooftop mass), or by increasing the rooftop mass, μ_i (for the same period T_i). However, these improvements are achieved in significantly different ways. On the one hand, increase of flexibility, T_i, leads to increased kinematics which engage more effectively the TMDI inerter and the damper while reduce forces developing at the isolators at the expense of larger isolator deflections. On the other hand, increase of rooftop mass reduce the deflection demands of the isolators, leading to reduced inerter forces, at the expense of larger isolation layer forces. In view of the above, it becomes evident that the stiffness and the mass properties of the isolated rooftop need to be carefully selected, accounting for practical considerations concerning the additional (rooftop) mass that can be accommodated, especially in existing buildings, and the required deformation demands that can be exhibited by the isolators without compromising their stability.

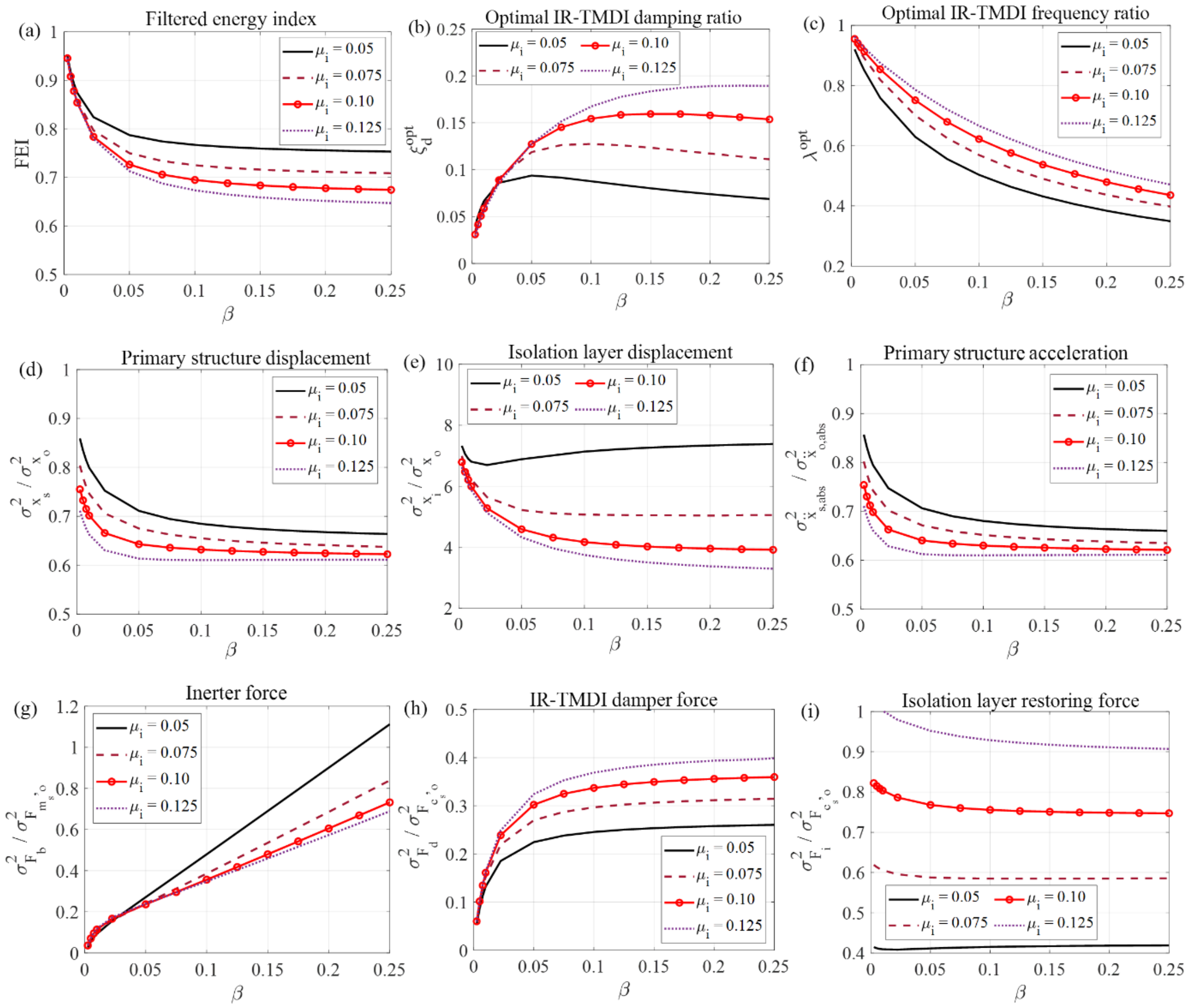

Fig. 4: *Optimal IR-TMDI properties using the FEI tuning criterion and normalized system response variances plotted against the inertance ratio for different isolated slab mass ratios μ_i and for T_s=1s, ξ_s=5%, T_i=3.5s, ξ_i=5%, μ_d=0.5%, white noise excitation with PGA=0.3g and ω_c=15π.*

Further to the isolators' stiffness and rooftop mass, the influence of the viscous damping ratio ξ_i of the isolation layer to the response of FEI-based tuned IR-TMDI is examined in Fig.5 whereby numerical data for three different ξ_i values are plotted while keeping ELS and excitation parameters the same as in the base case. It is found that by adopting low-damping bearings achieves lower FEI values (Fig.5(a)) and, consequently, better primary structure performance in terms of displacement (Fig.5(d)) and acceleration (Fig.5(f)). These improvements become consistently higher with inertance and are readily attributed to a better engagement of the TMDI through increased isolated rooftop kinematics/deflections (Fig.5(e)), similar to the case of reducing the stiffness of the isolators. In particular, lower isolation layer damping leads to higher TMDI inerter and damping forces and to lower shear force demands to the isolators. Interestingly, optimal TMDI frequency ratio is practically unaffected by changes to ξ_i, while optimal TMDI damping ratio reduces with ξ_i which further indicates that the increased damping forces and energy dissipation by the TMDI is due to larger kinematics (relative velocity) at the ends of the damping element. In this respect, it is evident that the use of low-damping isolators (i.e. isolators which require a reduced damping coefficient c_i for modelling their resisting force in Eq.(4)) is preferable as it allows for more seismic energy dissipation to take place by the TMDI damper element and increases the amplitude of the TMDI damping and inerter forces over the isolators' force.

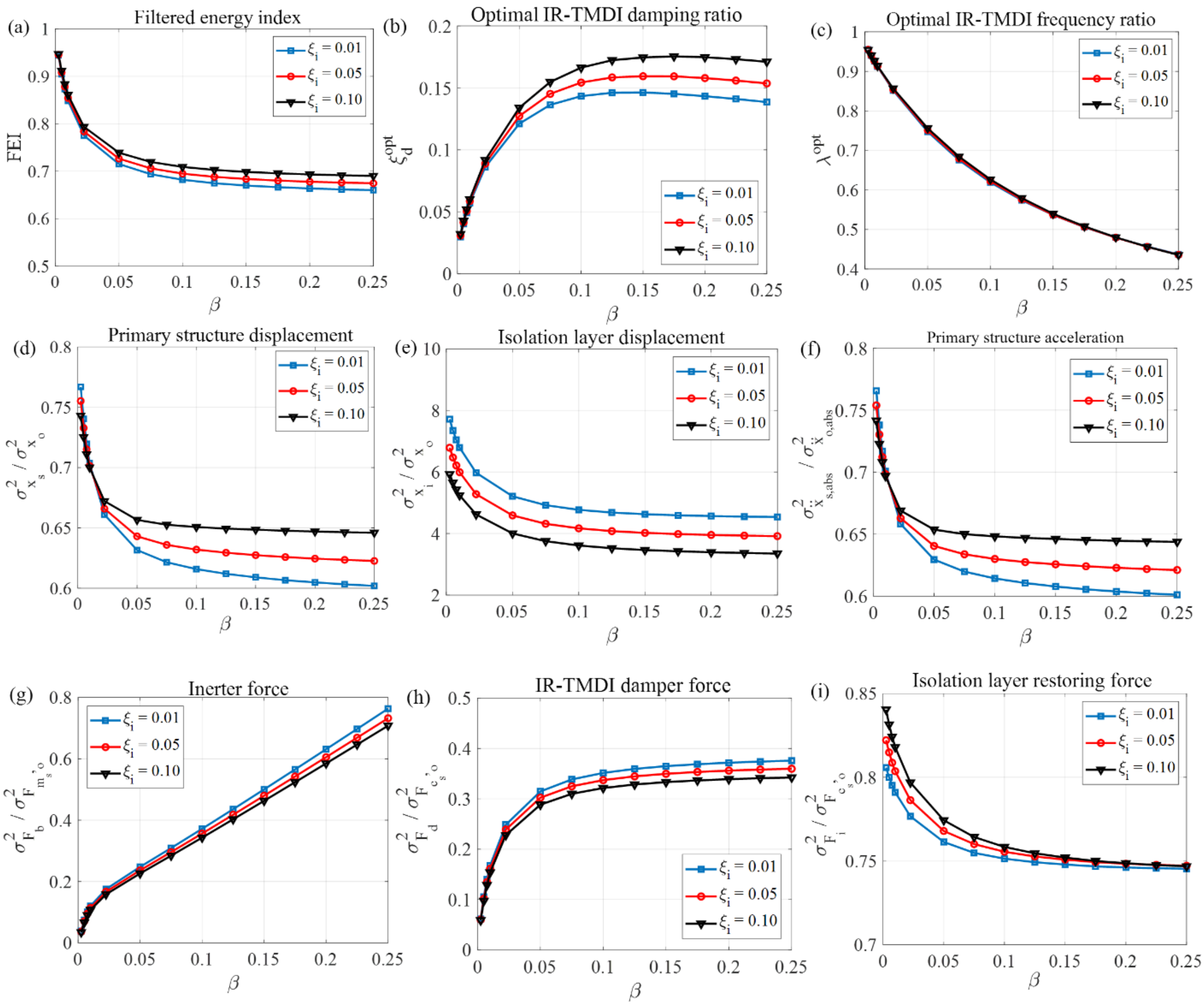

Fig. 5*: Optimal IR-TMDI properties using the FEI tuning criterion and normalized system response variances plotted against the inertance ratio for different isolated layer damping ratios ξ_i and for T_s=1s, ξ_s=5%, μ_i=10%, T_i=3.5s, ξ_i=5%, μ_d=0.5%, white noise excitation with PGA=0.3g and ω_c=15π.*

5.2 Influence of excitation properties

In this section, attention is focused on assessing the influence of the amplitude and frequency content of the stationary base excitation adopted for the IR-TMDI tuning to the seismic response of the ELSs. For this purpose, Fig.6 furnishes numerical data pertaining to the base case properties with 4 different PGA values corresponding to different white noise excitation intensities as per Eq.(19). Further, in Fig.7 data for the base case system under the two colored noise (Filtered Kanai-Tajimi) excitations with different frequency content defined in Table 1 for PGA=0.3g in Eq.(22) are compared to the data for white noise excitation with PGA= 0.3g. These colored noise excitations represent better the expected site-specific frequency content of seismic ground motions inasmuch as the local soil conditions are accurately captured by the Kanai-Tajimi filter parameters.

Examining first the variation of the excitation intensity in Fig.6, it is seen that the optimal TMDI damping ratio is rather sensitive to the assumed design PGA, which is not the case for the optimal TMDI frequency ratio in Fig.6(c). Importantly, the IR-TMDI becomes more efficient in reducing the primary structure response compared to the uncontrolled structure as PGA increases and for β>5%. This can be attributed to the larger isolation layer deflections induced by higher PGA excitation in Fig.6(e) which, in turn, engage better the TMDI as evidenced by the higher inerter and damping forces with PGA in Figs. 6(g) and 6(h), respectively. In this regime, the forces developed at the isolator reduce compared to the forces developed at the uncontrolled structure as PGA increases (Fig.6(i)) as a result of the increasingly important role of the TMDI in resisting seismic excitation with PGA.

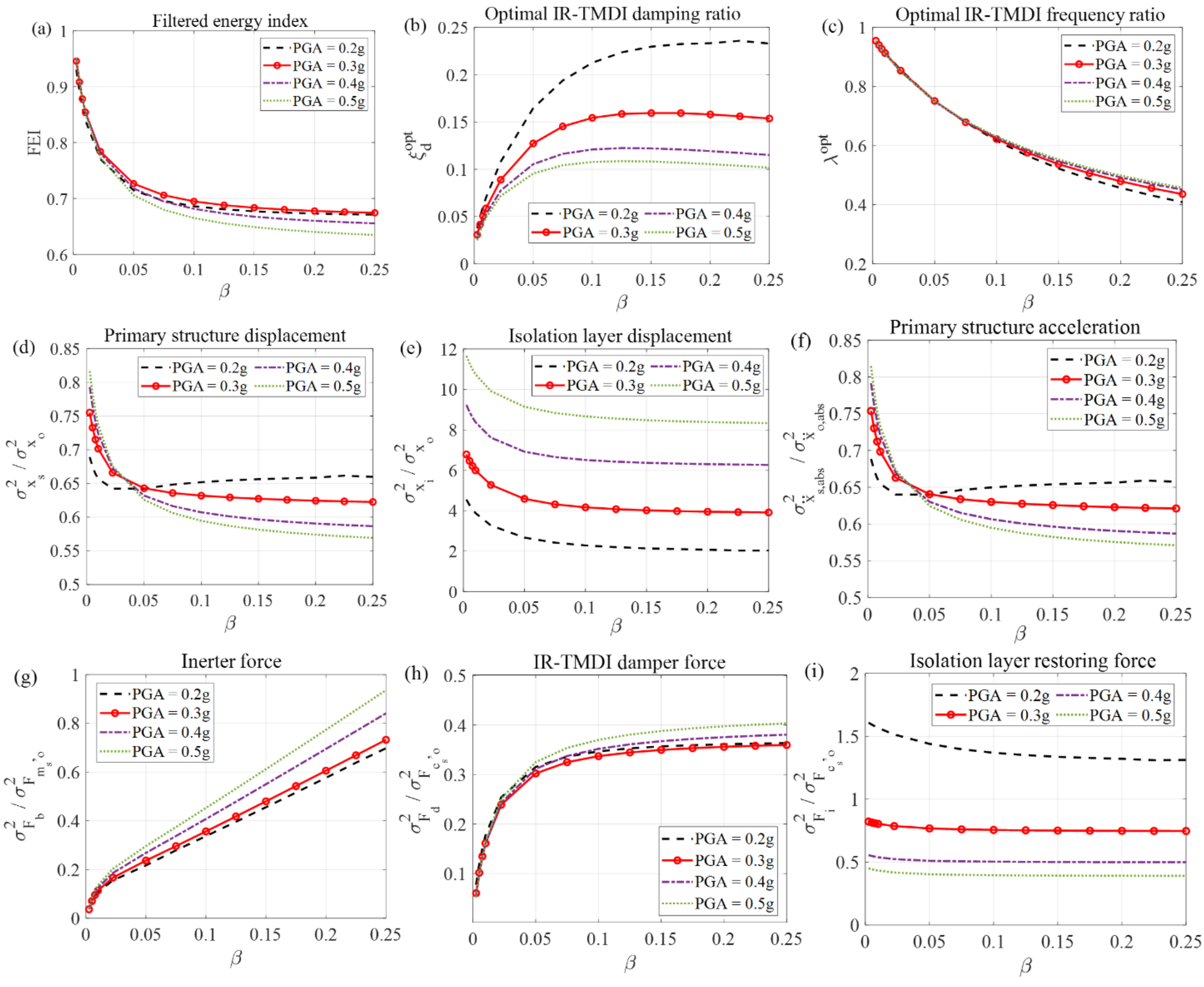

Fig. 6*: Optimal IR-TMDI properties using the FEI tuning criterion and normalized system response variances plotted against the inertance ratio for white noise excitation with different PGA values and ω_c=15π, and for T_s=1s, ξ_s=5%, μ_i=10%, T_i=3.5s, ξ_i=5%, μ_d=0.5%.*

Turning the attention to the data in Fig.7, it is seen that the frequency content of the seismic excitation does affect the optimal IR-TMDI tuning insofar as the optimal TMDI damping ratio in Fig.7(b) is significantly different for the colored noise excitations compared to the white noise excitation. Nevertheless, insignificant differences are observed in the TMDI frequency ratio and only for β>8% in Fig.7(c). Notably, the IR-TMDI suppresses appreciably the primary structure response in terms of both displacement and acceleration in Figs.7(d) and 7(f), respectively, for all the considered excitations. In all cases, higher improvements to the structural seismic performance are noted with increasing inertance, though the level of the improvements does depend on the frequency content of the excitation. The structural response reductions are due to higher TMDI inerter and damping forces developed as inertance increases, for all different types of excitations, as seen in Figs.7(g) and 7(h), respectively.

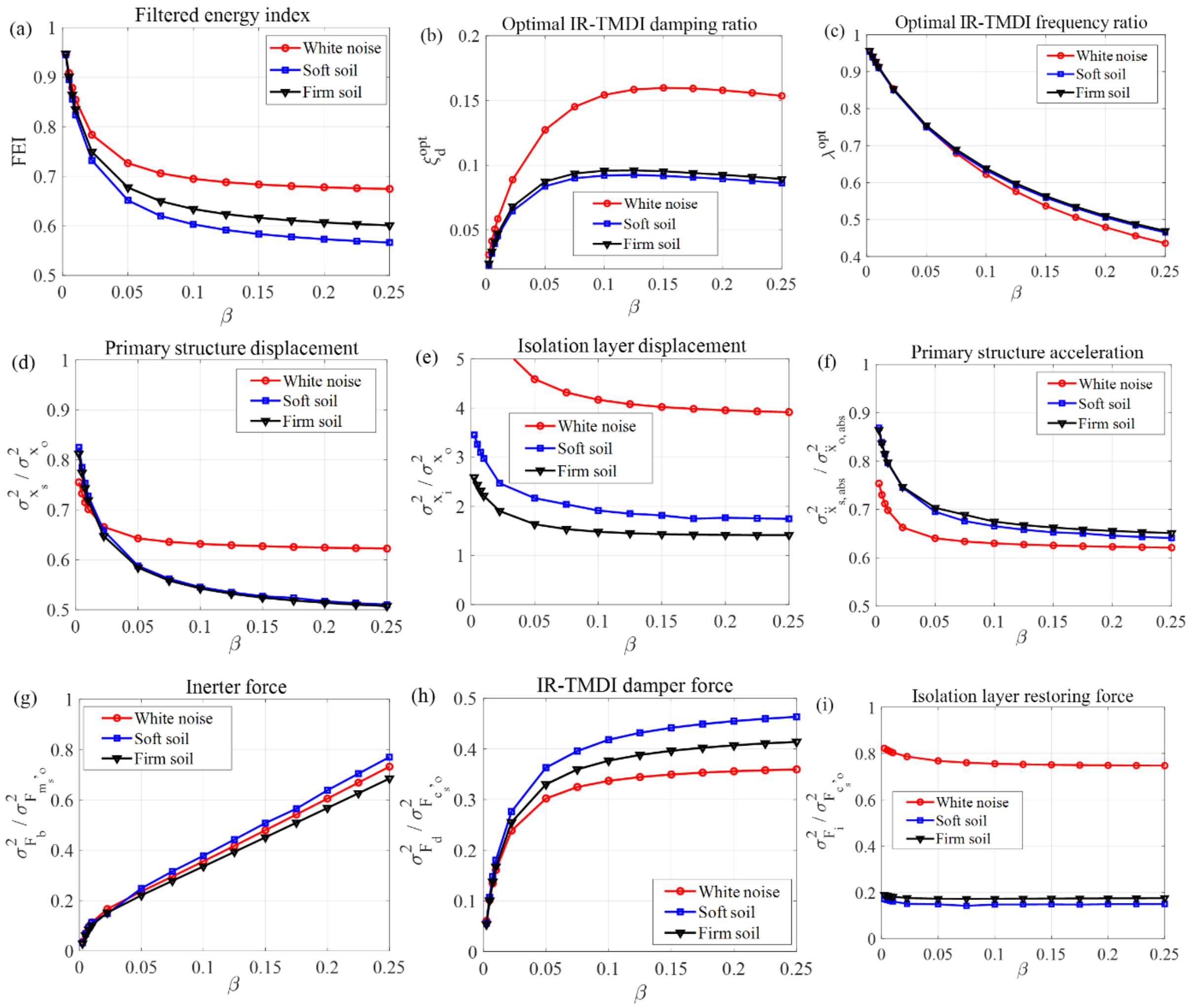

Fig. 7*: Optimal IR-TMDI properties using the FEI tuning criterion and normalized system response variances plotted against the inertance ratio for stationary excitations with different frequency content and PGA=0.3g and for T_s=1s, ξ_s=5%, μ_i=10%, T_i=3.5s, ξ_i=5%, μ_d=0.5%.*

Overall, the data in Fig.7 suggest that the frequency content of the excitation plays a major role to the system response. For instance, the colored noise excitations pose significantly lower deflection and resisting force demands to the isolators as seen in Figs.7(e) and 7(i). Further, the primary structure displacement response reductions in Fig.7(d) are consistently higher for the colored noise excitations compared to white noise excitation, while the opposite holds for the structural acceleration reductions in Fig.7(f). Nevertheless, the observed differences between colored and white noise excitations are dependent on the proximity of the natural period of the primary structure, T_s, with the dominant period of the colored excitations reported in Table 1. To investigate the latter point, as well as to gauge the influence of the primary structure to the IR-TMDI tuning and structural response mitigation potential, Fig.8 furnishes "response spectra" by plotting all 9 quantities examined in Figs.2-7 for the three different excitations considered in Fig.7 and inertance ratio β=20% for different structural natural period T_s. It is seen that the optimal TMDI parameters in Figs.8(b) and (c) do not depend much on the dominant frequency of the colored noise excitation, though there are significant differences between white noise and colored noise excitations for T_s>0.6s. Importantly, the trends and observations made in view of the data in Fig.7 on the differences between white and colored noise are valid for all different primary structures with 0.6s<T_s<1.8s. Specifically, higher primary structure displacement reductions are achieved for colored noise excitation vis-à-vis white noise excitation, except for the relatively stiff primary structures with T_s<0.6s (Fig. 8(d)), while the opposite holds for structural response acceleration (Fig. 8(f)). Further, higher deflection demands at the isolators are observed for white noise vis-à-vis colored noise which, though, reduce as the primary structure flexibility increases (Fig.8(e)). Moreover, the lower FEI ordinates in Fig.8(a) achieved by optimal tuning under different excitations reflect on consistently larger damping forces (Fig.8(g)) for the full range of primary structures considered. Further, the isolator force demands remain significantly lower for the colored noise vis-à-vis white noise, again for all primary structures (Fig.8(i)).

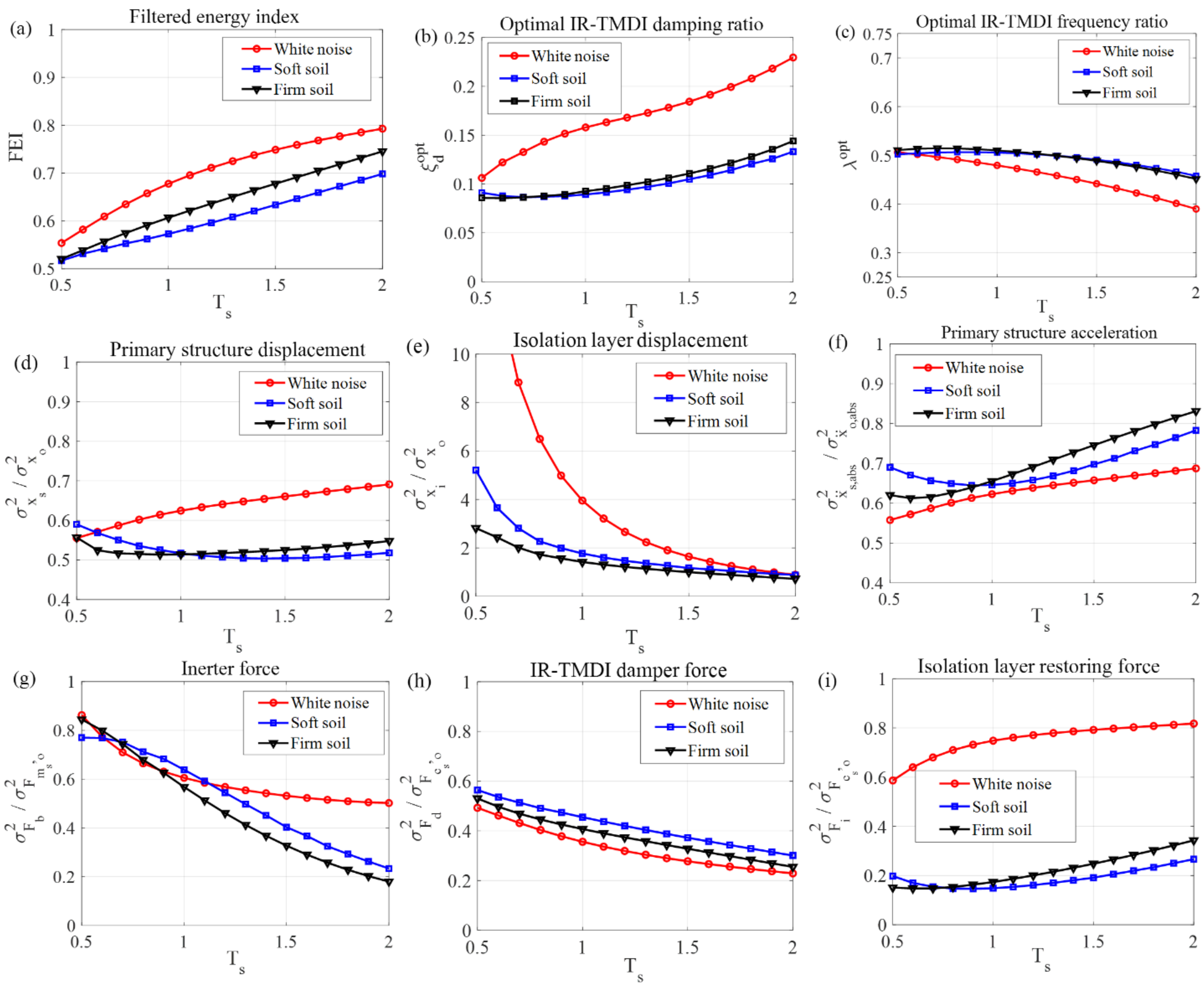

Fig. 8: *Response spectra of optimal IR-TMDI properties using the FEI tuning criterion for stationary excitations with different frequency content and PGA=0.3g and for ξ_s=5%, μ_i=10%, T_i=3.5s, ξ_i=5%, μ_d=0.5% and β=20%.*

6 Verification of IR-TMDI effectiveness using nonlinear response history analysis

In previous Sections, the response of the ELS in Eq.(4) under stationary excitations has been used as a proxy to appraise the effectiveness of the optimal IR-TMDI for primary structure seismic response mitigation. However, the response of IR-TMDI equipped structures to earthquake excitation is nonlinear and non-stationary due to the presence of the nonlinear isolators and the non-stationary amplitude and frequency content of naturally occurring seismic ground motions (GMs). To this end, it is herein deemed important to verify the IR-TMDI potential for structural seismic response mitigation by application of response history analyses to the nonlinear system equations in Eqs. (5) and (8) subject to recorded GMs. For this purpose, the base case system is considered equipped with the stiffest (T_i= 2.7s) and the most flexible (T_i= 4s) FEI-based optimally tuned IR-TMDIs previously studied in Fig.3.

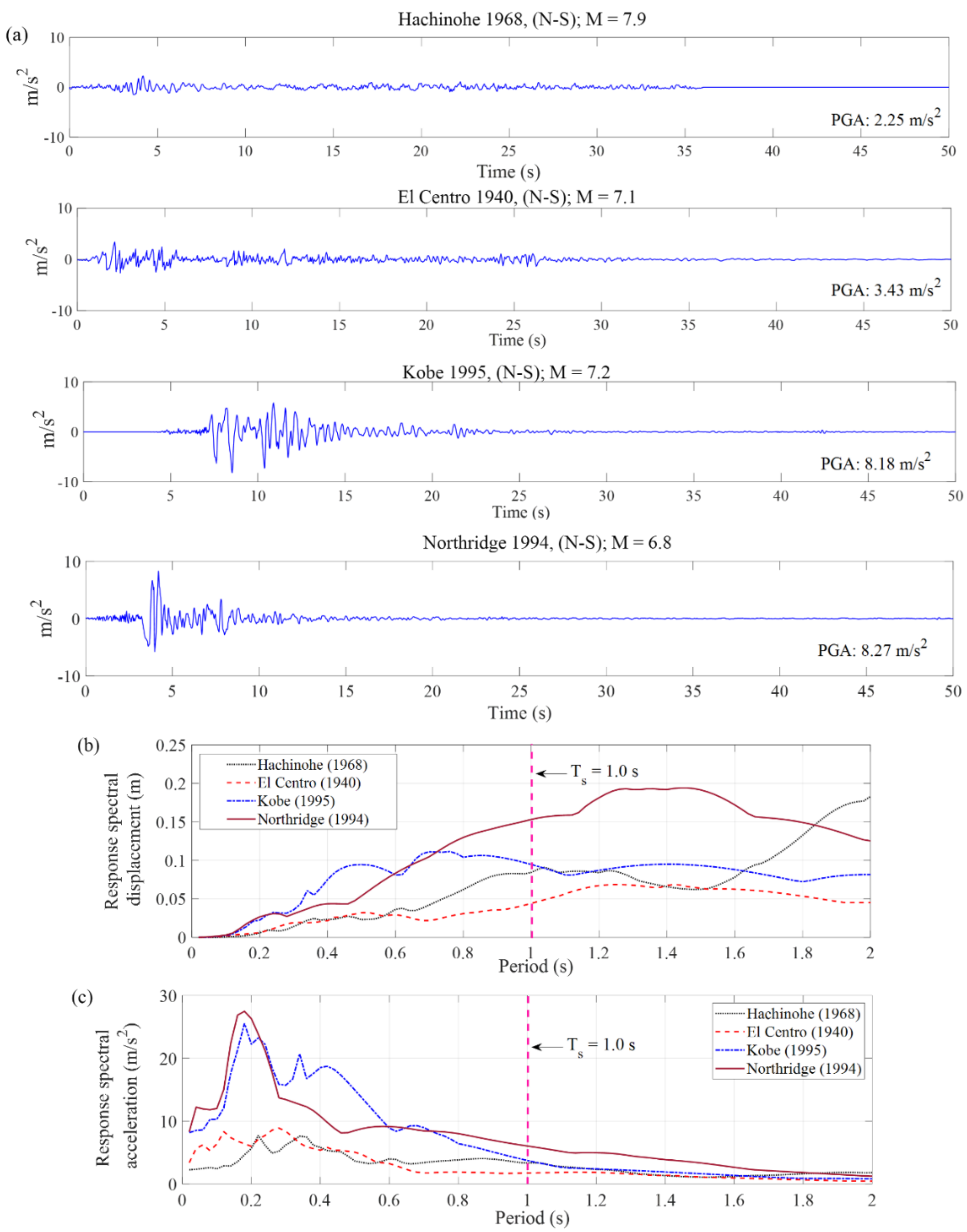

Fig. 9*: Considered recorded ground motions: (a) Time-histories, (b) Response spectral displacement for 5% damping ratio, (c) Response spectral acceleration for 5% damping ratio.*

For numerical implementation, a common nominal yielding displacement u_y=2cm is taken for the isolators while the normalized yielding strengths are set equal to 11% and 5% for the stiff and for the flexible isolators, respectively. Nonlinear response history analysis (NRHA) is undertaken for the 4 recorded GMs in Fig.9(a). These GMs are specified in Ohtori et al (2004) as part of a benchmark structural vibration control testbed problem. The El Centro and the Hachinohe records are far-field GMs, while the Northridge and the Kobe records are near-field GMs (see Ohtori et al 2004 for further details). Relative displacement and pseudo-acceleration response spectra of the GMs are shown in Figs.9(b) and 9(c) in which the T_s natural period of the primary structure is indicated. The as-recorded GMs in Fig.9(a) are herein scaled to PGA=0.3g which has been assumed in the IR-TMDI optimal tuning. Time-domain numerical integration of the nonlinear equations of motion is performed in MATLAB using the standard `ode45` solver.

Structural response time-histories in terms of relative displacement and absolute acceleration are plotted in Fig. 10 for the two considered IR-TMDI equipped structures subject to the four GMs in Fig.9. To facilitate the appraisal of the IR-TMDI structural response mitigation potential with different T_i, the time-histories in each panel are normalized with respect to the highest absolute response of the uncontrolled primary structure whose response time-history is also plotted. Moreover, Table 2 provides the peak absolute and root-mean-square (RMS) displacement and acceleration response reductions achieved by the two different IR-TMDIs for each GM as well as their average value across the four GMs. Data in Fig.10 and Table 2 verify the trends observed and discussed in Section 5 in terms of the RMS values: despite the record-to-record variability, the IR-TMDI reduces appreciably RMS structural displacement and acceleration for each GM individually and, therefore, on the average. Reductions in terms of RMS acceleration is slightly by consistently higher than reduction in RMS displacement for all GMs and systems, while the IR-TMDI with the more flexible isolators performing significantly better for each GM. More importantly, similar observations are made for the peak response values, with the exception of the Northridge GM for which the peak displacement response of primary structure is 4% higher from the uncontrolled structure when equipped with the IR-TMDI with stiff isolators (T_i= 2.7s), while shows no improvement when equipped with the IR-TMDI with flexible isolators (T_i= 4s). This inability of the IR-TMDI to suppress the peak structural displacement for the Northridge GM is because the record begins with one early large pulse with long period under which the primary structure attains each peak response before the IR-TMDI is activated kinematically (i.e. moves with respect to the primary structure) to produce resisting inerter and damping forces and to dissipate energy. This is a well-reported in the literature disadvantage common to all inertial vibrations absorbers, including the TMDI (De Angelis et al. 2019). Still, the IR-TMDI does reduce the peak structural acceleration even for the Northridge GM, while the IR-TMDI with flexible isolators reduces the average peak structural displacement response from all the considered GMs by 20%.

Table 2: Peak and RMS values of the normalized response time-histories of Fig.10

	Peak absolute response				RMS response			
	T_i = 2.7s		T_i = 4.0s		T_i = 2.7s		T_i = 4.0s	
	displ.	acc.	displ.	acc.	displ.	acc.	displ.	acc.
Hachinohe	0.71	0.66	0.70	0.67	0.64	0.58	0.52	0.48
El Centro	0.76	0.70	0.63	0.59	0.78	0.71	0.68	0.64
Northridge	1.04	0.95	1.00	0.90	0.91	0.83	0.83	0.75
Kobe	0.89	0.83	0.87	0.83	0.61	0.56	0.54	0.51
Mean values	0.85	0.78	0.80	0.75	0.73	0.67	0.64	0.60

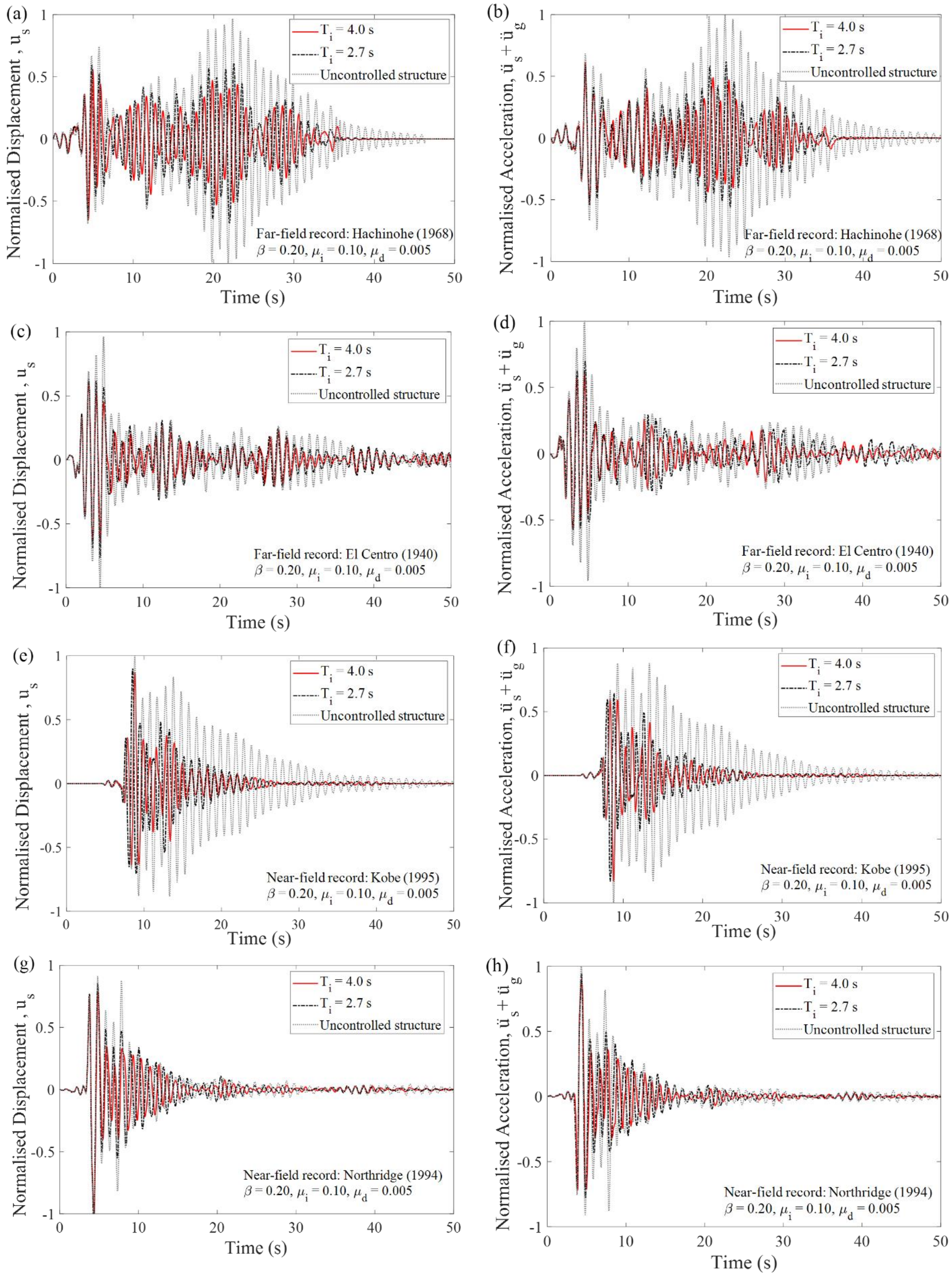

Fig. 10: *Primary structure response time-histories normalized to the peak absolute response of the uncontrolled structure for the GMs in Fig.9.*

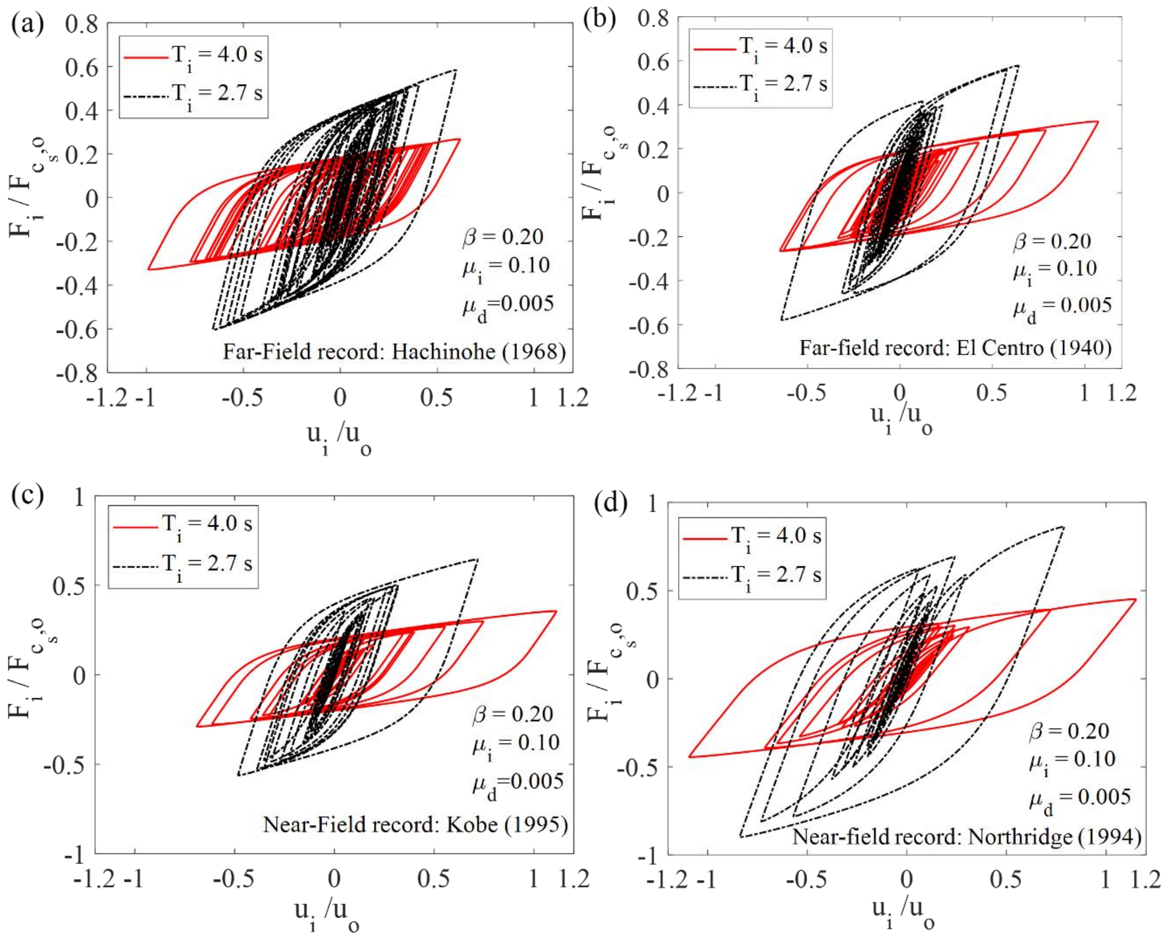

Fig. 11*:* Isolators' force-deformation plots *for the GMs in Fig.9.*

Finally, Fig.11 plots the force-deformation curves (hysteretic loops) of the isolators for both the IR-TMDI equipped structures considered under the GMs in Fig.9. The plots are normalized with respect to the peak damping force and structural displacement of the uncontrolled primary structure. These data confirm that the IR-TMDI with more flexible isolators exhibits higher deflections than the stiffer isolators which, in turn, activate more effectively the TMDI, resulting in higher structural response reductions (Table 1). Evidently, the higher resisting forces developed by the stiffer isolators are not as effective as the action of the FEI-based optimally tuned TMDI in mitigating the seismic response of the primary structure. Clearly, this observation establishes the potential of the IR-TMDI for efficient seismic protection of structures, provided that a judicial selection of the isolators' stiffness in conjunction with FEI-based IR-TMDI tuning are adopted.

7 Concluding remarks

Motivated by the insight that the TMDI vibration suppression capability improves by increasing the structural flexibility between the floors it is attached to, a novel passive energy dissipation system, IR-TMDI, comprising a TMDI contained within a seismically isolated rooftop, has been herein proposed and its potential for the seismic protection of buildings has been numerically demonstrated. The intended working principle of the IR-TMDI is to improve the structural seismic response mitigation effectiveness of the TMDI through the creation of a phenomenologically flexible floor achieved upon yielding of the isolation layer under severe ground motions.

This intended functionality of the IR-TMDI has been numerically verified by considering a nonlinear mechanical model whereby a low-fidelity damped single mode representation was adopted for the primary structure, while the yielding isolators were represented by the Bouc-Wen hysteretic model. The verification has been supported by an equivalent linear system (ELS), derived through statistical linearization, which expedited the optimal IR-TMDI tuning for vairous isolated rooftop properties, inertance, and primary structure natural periods under white noise excitations with different intensities as well as Kanai-Tajimi excitations with different frequency content corresponding to soft and firm soil conditions.

It was established that tuning for maximizing TMDI seismic energy dissipation (FEI-based tuning) is more advantageous than tuning for minimizing primary structure displacement or acceleration response, as it lowers deflection and force demands to the isolators as well as the inerter force. Moreover, significant primary structure displacement and acceleration reductions are achieved as the effective rooftop flexibility increases, through reduction of the nominal strength of the isolators, which verifies the intended working principle of the IR-TMDI. This was further confirmed from numerical data pertaining to nonlinear response history analyses under four benchmark recorded ground motions. Furthermore, for IR-TMDI with sufficiently flexible isolators (i.e. three times more flexible than the primary structure), improved seismic structural performance with concurrent reduced deflection and force demands at the isolators is shown for all considered stationary excitations as the inertance scales-up, which is readily achievable technologically. Additional conclusions drawn from the parametric study are that the use of higher damping isolators is detrimental to the primary structure response, larger relative structural response improvements are achieved for higher seismic intensity (PGA), and that the relative improvement in structural accelerations reduce as well as the deflection demands at the isolators for stiffer primary structures.

Lastly, it was noted that improved structural seismic performance concurrently with reduced the deflection demands at the isolators is also achieved by increasing the rooftop mass for fixed inertance and effective isolation period. Nevertheless, these improvements come at the cost of significantly higher isolator forces to be transferred to the structure, further to the increased weight that the isolators and the primary structure need to accommodate. In this regard, whilst a detailed consideration of practical technological aspects and implementation of the proposed IR-TMDI falls outside the scope of this work, the increase of rooftop mass is likely to be a least attractive approach to improve IR-TMDI performance compared to reducing isolation natural period in practice, especially for existing structures. Still, it is noted that the combination of relatively lightweight rooftops with large deformation demands and low vertical loads may become detrimental to the stability of elastomeric bearings. However, applications of lightweight base isolated residential houses and timber buildings as discussed by Ryan and Earl (2010) as well as partial isolation in multi-storey buildings (Faiella and Mele 2020) support the practical feasibility of IR-TMDI. To this aim, further research is warranted involving the detailed design and assessment of IR-TMDI for benchmark/case-study multistorey buildings which is left for future work. Ultimately, this consideration will further reinforce and quantify the herein established advantages of the IR-TMDI over TMDI configurations spanning several floors, widely considered in the recent literature, rendering the IR-TMDI particularly applicable to the bulk of buildings in high seismicity areas, that is, low-to-mid-rise new-built and existing structures.

Acknowledgements

The first author gratefully acknowledges the financial support from the School of Science and Technology at City, University of London through a fully funded PhD studentship.

Appendix A: Energy dissipation index derivation

In this Appendix, the energy-based performance criterion in Eq.(24) is derived. To this aim, the equations of motion of the ELS in Eq.(16) are first written as

$$m_s\ddot{x}_s + c_s\dot{x}_s + k_s x_s - \left(c_i\left(\dot{x}_{is}-\dot{x}_s\right) + \alpha k_i\left(x_{is}-x_s\right) + (1-\alpha)F_y y\right) - b\left(\ddot{x}_d - \ddot{x}_s\right) = -m_s\ddot{x}_g \tag{A.1a}$$

$$m_i\ddot{x}_{is} + c_i\left(\dot{x}_{is}-\dot{x}_s\right) + \alpha k_i\left(x_{is}-x_s\right) + (1-\alpha)F_y z - \left(c_d\left(\dot{x}_d-\dot{x}_{is}\right) + k_d\left(x_d-x_{is}\right)\right) = -m_i\ddot{x}_g \tag{A.1b}$$

$$m_d\ddot{x}_d + c_d\left(\dot{x}_d-\dot{x}_{is}\right) + k_d\left(x_d-x_{is}\right) + b\left(\ddot{x}_d-\ddot{x}_s\right) = -m_d\ddot{x}_g \tag{A.1c}$$

Next, the so-called equations of relative energy balance are derived by multiplying Eq. (A1a) by $\dot{x}_s$, Eq. (A1b) by $\dot{x}_{is}$ and Eq. (A1c) by $\dot{x}_d$ and integrating over time to yield (e.g. Uang & Bertero 1988)

$$E_{m_s}(t) + E_{c_s}(t) + E_{k_s}(t) - E_{c_{i,s}}(t) - E_{k_{i,s}}(t) - E_{h_{i,s}}(t) - E_{b,s}(t) = E_{g_s}(t) \tag{A.2a}$$

$$E_{m_i}(t) + E_{c_i}(t) + E_{h_i}(t) + E_{k_i}(t) - E_{c_{d,is}}(t) - E_{k_{d,is}}(t) = E_{g_i}(t) \tag{A.2b}$$

$$E_{m_d}(t) + E_{c_d}(t) + E_{k_d}(t) + E_b(t) = E_{g_d}(t) \tag{A.2c}$$

In Eq.(A.2a), E_{m_s}, E_{c_s} and E_{k_s} are the kinetic energy, viscous damping energy, and elastic strain energy of the primary structure, respectively, given by

$$E_{m_s}(t) = m_s\int_0^t \ddot{x}_s\dot{x}_s \mathrm{d}t, \quad E_{c_s}(t) = c_s\int_0^t \dot{x}_s^2 \mathrm{d}t, \text{ and } E_{k_s}(t) = k_s\int_0^t x_s\dot{x}_s \mathrm{d}t \;, \tag{A.3}$$

$E_{c_{i,s}}$, $E_{k_{i,s}}$ and $E_{h_{i,s}}$ are the viscous damping energy, strain energy, and hysteretic dissipated energy transferred from the isolation system to the primary structure, respectively, given by

$$\begin{aligned} &E_{c_{i,s}}(t) = -c_i\int_0^t \dot{x}_s^2 \mathrm{d}t + c_i\int_0^t \dot{x}_{is}\dot{x}_s \mathrm{d}t, \quad E_{k_{i,s}}(t) = -\alpha k_i\int_0^t x_s\dot{x}_s \mathrm{d}t + \alpha k_i\int_0^t x_{is}\dot{x}_s \mathrm{d}t, \quad \text{and} \\ &E_{h_{i,s}}(t) = (1-\alpha)k_i u_y\int_0^t y\dot{x}_s \mathrm{d}t, \end{aligned} \tag{A.4}$$

$E_{b,s}$ is the energy transferred from the inerter to the primary structure, given by

$$E_{b,s}(t) = -b\int_0^t \ddot{x}_s\dot{x}_s \mathrm{d}t + b\int_0^t \ddot{x}_d\dot{x}_s \mathrm{d}t \;, \tag{A.5}$$

and E_{g_s} is the seismic excitation energy entering the primary structure, given by

$$E_{g_s}(t) = -m_s\int_0^t \ddot{x}_g\dot{x}_s \mathrm{d}t \tag{A.6}$$

Further, in Eq.(A.2b), E_{m_i}, E_{c_i}, E_{k_i} and E_{h_i} are the kinetic energy, viscous damping energy, elastic strain energy and hysteretic energy dissipation of the isolated rooftop, respectively, given by

$$\begin{aligned}&E_{m_i}(t)=m_i\int_0^t \ddot{x}_{is}\dot{x}_{is}\mathrm{d}t,\quad E_{c_i}(t)=c_i\int_0^t \dot{x}_{is}^2\mathrm{d}t-c_i\int_0^t \dot{x}_s\dot{x}_{is}\mathrm{d}t,\\&E_{k_i}(t)=\alpha k_i\int_0^t x_{is}\dot{x}_{is}\mathrm{d}t-\alpha k_i\int_0^t x_s\dot{x}_{is}\mathrm{d}t\quad\text{and}\quad E_{h_i}(t)=(1-\alpha)k_i u_y\int_0^t y\dot{x}_{is}\mathrm{d}t,\end{aligned}\tag{A.7}$$

$E_{c_{d,is}}$ and $E_{k_{d,is}}$ are the damping element energy and spring energy transferred from the TMDI to the isolated rooftop, respectively, given by

$$E_{c_{d,is}}(t)=-c_d\int_0^t \dot{x}_{is}^2\mathrm{d}t+c_d\int_0^t \dot{x}_d\dot{x}_{is}\mathrm{d}t\quad\text{and}\quad E_{k_{d,is}}(t)=-k_d\int_0^t x_{is}\dot{x}_{is}\mathrm{d}t+k_d\int_0^t x_d\dot{x}_{is}\mathrm{d}t,\tag{A.8}$$

and E_{g_i} is the seismic excitation energy entering the isolated floor system, given by

$$E_{g_i}(t)=-m_i\int_0^t \ddot{x}_g\dot{x}_{is}\mathrm{d}t\tag{A.9}$$

In addition, in Eq.(A.2b), E_{m_d}, E_{c_d}, E_{k_d} and E_b are the kinetic energy, viscous damping energy, elastic strain energy, and inerter energy of the TMDI, respectively, given by

$$\begin{aligned}&E_{m_d}(t)=m_d\int_0^t \ddot{x}_d\dot{x}_d\mathrm{d}t,\quad E_{c_d}(t)=c_d\int_0^t \dot{x}_d^2\mathrm{d}t-c_d\int_0^t \dot{x}_{is}\dot{x}_d\mathrm{d}t,\\&E_{k_d}(t)=k_d\int_0^t x_d\dot{x}_d\mathrm{d}t-k_d\int_0^t x_{is}\dot{x}_d\mathrm{d}t,\quad\text{and}\quad E_b(t)=b\int_0^t \ddot{x}_d\dot{x}_d\mathrm{d}t-b\int_0^t \ddot{x}_s\dot{x}_d\mathrm{d}t,\end{aligned}\tag{A.10}$$

and E_{g_d} is the seismic excitation energy entering the TMDI, given by

$$E_{g_d}(t)=-\int_0^t m_d\ddot{x}_g\dot{x}_d\mathrm{d}t\,.\tag{A.11}$$

Assuming Gaussian stationary stochastic seismic excitation and taking the mathematical expectation in both sides of Eqs. (A.2), the following set of equations are derived in a small increment of time Δt under ergodic conditions (see also Pietrosanti et al. 2017)

$$\begin{aligned}&E\left[\Delta E_{g_s}\right]=E\left[\Delta E_{m_s}\right]+E\left[\Delta E_{c_s}\right]+E\left[\Delta E_{k_s}\right]-E\left[\Delta E_{c_{i,s}}\right]-E\left[\Delta E_{k_{i,s}}\right]-E\left[\Delta E_{h_{i,s}}\right]-E\left[\Delta E_{b,s}\right]\\&E\left[\Delta E_{g_i}\right]=E\left[\Delta E_{m_i}\right]+E\left[\Delta E_{c_i}\right]+E\left[\Delta E_{h_i}\right]+E\left[\Delta E_{k_i}\right]-E\left[\Delta E_{c_{d,is}}\right]-E\left[\Delta E_{k_{d,is}}\right]\\&E\left[\Delta E_{g_d}\right]=E\left[\Delta E_{m_d}\right]+E\left[\Delta E_{c_d}\right]+E\left[\Delta E_{k_d}\right]+E\left[\Delta E_b\right]\end{aligned}\tag{A.12}$$

In Eq.(A.12) the following incremental energy terms vanish $E\left[\Delta E_{m_s}\right]=E\left[\Delta E_{m_i}\right]=E\left[\Delta E_{m_d}\right]=E\left[\Delta E_{k_s}\right]=0$ due to the property $E[u\dot{u}]=0$ which holds for any Gaussian temporal stochastic process *u* (e.g. Roberts & Spanos 2003). Further, it can be shown that $E\left[\Delta E_{k_i}\right]-E\left[\Delta E_{k_{i,s}}\right]+E\left[\Delta E_{k_d}\right]-E\left[\Delta E_{k_{d,is}}\right]+E\left[\Delta E_b\right]-E\left[\Delta E_{b,s}\right]=0$ by making use of the previous property together with the coordinate transformations $x_i = x_{is} - x_s$ and $x_k = x_d - x_{is}$ and some algebraic manipulation. To this end, by summing the three expressions in Eq.(A.12), the total expected incremental seismic input energy in the ELS system $E[\Delta E_{Total}]$ is found as

$$E\left[\Delta E_{Total}\right]=E\left[\Delta E_{g_s}\right]+E\left[\Delta E_{g_i}\right]+E\left[\Delta E_{g_d}\right]= c_s\sigma^2_{\dot{x}_s}\Delta t+c_d\sigma^2_{\dot{x}_k}\Delta t+c_i\sigma^2_{\dot{x}_i}\Delta t+\left(1-\alpha\right)k_iu_y\sigma^2_{y\dot{x}_i}\Delta t, \tag{A.13}$$

by noting that

$$\begin{aligned}
&E\left[\Delta E_{c_s}\right]=c_sE\left[\dot{x}_s^2\right]\Delta t=c_s\sigma^2_{\dot{x}_s}\Delta t,\quad E\left[\Delta E_{c_i}\right]-E\left[\Delta E_{c_{i,s}}\right]=c_iE\left[\left(\dot{x}_s-\dot{x}_{is}\right)^2\right]\Delta t=c_i\sigma^2_{\dot{x}_i}\Delta t,\\
&E\left[\Delta E_{c_d}\right]-E\left[\Delta E_{c_{d,is}}\right]=c_dE\left[\left(\dot{x}_d-\dot{x}_{is}\right)^2\right]\Delta t=c_d\sigma^2_{\dot{x}_k}\Delta t,\quad and\\
&E\left[\Delta E_{h_i}\right]-E\left[\Delta E_{h_{i,s}}\right]=\left(1-\alpha\right)k_iu_yE\left[y\left(\dot{x}_{is}-\dot{x}_s\right)\right]\Delta t=\left(1-\alpha\right)k_iu_y\sigma^2_{y\dot{x}_i}\Delta t
\end{aligned} \tag{A.14}$$

Finally, the energy dissipation index (EDI) defined by Pietrosanti et al. (2017) as the ratio of the energy dissipated by the TMDI damping element over the total input energy is given as

$$EDI=\frac{E\left[\Delta E_{c_d}\right]-E\left[\Delta E_{c_{d,is}}\right]}{E\left[\Delta E_{Total}\right]} \tag{A.15}$$

for the herein considered ELS. Then, Eq.(24) follows from Eqs.(A.13)-(A.15).

References

Berquist, M., De Pasquale, R., Frye, S., Gilani, A., Klembczyk, A., Lee, D., Malatesta, A., Metzger, J., Schneide, R., Smith, C., Taylor, D., Wang, S. & Winters, C. (2019). Fluid Viscous Dampers General Guidelines for Engineers Including a Brief History. Taylor Devices, Inc: New York.

Brzeski, P., Lazarek, M. & Perlikowski, P. (2017). Experimental study of the novel Tuned Mass Damper with inerter which enables changes of inertance. Journal of Sound and Vibration, 404, 47–57. https://doi.org/10.1016/j.jsv.2017.05.034

Brzeski, P. & Perlikowski, P. (2017). Effects of play and inerter nonlinearities on the performance of tuned mass damper. Nonlinear Dynamics, 88, 1027- 1041.

Clough, R. & Penzien, J. (2003). Dynamics of structures, 2nd Edition. Mc Graw-Hill, NY.

Charles, A. & Dennis, Jr JE. (2008). Analysis of generalized pattern searches. SIAM Journal on Optimization, 13, 889–903.

Colherinhas, B.G., Petrini, F., De Morais, M.V.G. & Bontempi F. (2021). Optimal design of passive-adaptive pendulum tuned mass damper for the global vibration control of offshore wind turbines. Wind Energy, 24: 573–595. DOI: 10.1002/we.2590.

Dai, J., Xu, Z. & Gai, P. (2019). Tuned mass-damper-inerter control of wind-induced vibration of flexible structures based on inerter location. Engineering Structures, 199, 109585.

De Angelis, M., Perno, S. & Reggio, A. (2011). Dynamic response and optimal design of structures with large mass ratio TMD. Earthquake Engineering & Structural Dynamics, 41(1), 41–60. https://doi.org/10.1002/eqe.1117

De Angelis, M., Giaralis, A., Petrini, F. & Pietrosanti, D. (2019). Optimal tuning and assessment of inertial dampers with grounded inerter for vibration control of seismically excited base-isolated systems. Engineering Structures, 196, 109250.

De Domenico, D. & Ricciardi, G. (2018). Optimal design and seismic performance of tuned mass damper inerter (TMDI) for structures with nonlinear base isolation systems. Earthquake Engineering & Structural Dynamics, 47, 2539–2560. https://doi.org/10.1002/eqe.3098.

De Domenico, D., Ricciardi, G. & Zhang R. (2020). Optimal design and seismic performance of tuned fluid inerter applied to structures with friction pendulum isolators Soil Dynamics and Earthquake Engineering, 132, 106099.

Djerouni, S., Ounis, A., Elias, S., Abdeddaim, M. & Rupakhety, R. (2022). Optimization and performance assessment of tuned mass damper inerter systems for control of buildings subjected to pulse-like ground motions, Structures, 38, 139-156.

Elias, S. & Matsagar, V. (2017). Research developments in vibration control of structures using passive tuned mass dampers. Annual Reviews in Control, 44, 129–156. https://doi.org/10.1016/j.arcontrol.2017.09.015

Faiella, D. & Mele, E. (2019). Vibration characteristics and higher mode coupling in intermediate isolation systems (IIS): a parametric analysis. Bulletin of Earthquake Engineering, 17, 4347-4387.

Faiella, D. & Mele, E. (2020). Insights into inter-story isolation design through the analysis of two case studies. Engineering Structures, 215, 110660.

Freddi, F., Galasso, C., Cremen, G., Dall'Asta, A., Di Sarno, L., Giaralis, A., Gutiérrez-Urzúa, F., Málaga-Chuquitaype, C., Mitoulis, S.A., Petrone, C., Sextos, A., Sousa, L., Tarbali, K., Tubaldi, E., Wardman, J. & Woo, G. (2021). Innovations in earthquake risk reduction for resilience: recent advances and challenges. International Journal of Disaster Risk Reduction, 60, 102267.

Giaralis, A. & Spanos, P. (2012). Derivation of response spectrum compatible non-stationary stochastic processes relying on Monte Carlo-based peak factor estimation. Earthquakes and Structures, 3(5), 719-747. https://doi.org/10.12989/eas.2012.3.5.719.

Giaralis, A. & Petrini, F. (2017). Wind-induced vibration mitigation in tall buildings using the tuned mass-damper-inerter (TMDI). Journal of Structural Engineering, ASCE, 143(9): 04017127.,

Giaralis, A. & Taflanidis, A. A. (2018). Optimal tuned mass-damper-inerter (TMDI) design for seismically excited MDOF structures with model uncertainties based on reliability criteria. Structural Control and Health Monitoring, 25(2). https://doi.org/10.1002/stc.2082

Gonzales-Buelga, A., Lazar, I.F., Jiang, J.Z., Neild, S.A. & Inman, D.J. (2017). Assessing the effect of nonlinearities on the performance of a tuned inerter damper. Structural Control and Health Monitoring, 24, e1879.

Jangid, R. S. (2010). Stochastic response of building frames isolated by lead-rubber bearings. Structural Control and Health Monitoring, 17(1), 1–22. https://doi.org/10.1002/stc.266.

Javidialesaadi, A. & Wierschem, N.E. (2019). An inerter-enhanced nonlinear energy sink. Mechanical Systems and Signal Processing, 129, 449-454.

Ikhouane, F., Rodellar, J. & Hurtado, J.E. (2006). Analytical characterization of hysteresis loops described by the Bouc-Wen model. Mechanics of Advanced Materials and Structures, 13, 463–472.

Kaveh, A., Fahimi Farzam, M. & Hojat Jalali, H. (2020). Statistical seismic performance assessment of tuned mass damper inerter. Structural Control and Health Monitoring, 27(10). https://doi.org/10.1002/stc.2602

Li, Q.S., Zhi, L.H., Tuan, A.Y., Kao, C.S., Su, S.C. & Wu, C.F. (2011). Dynamic Behavior of Taipei 101 Tower: Field Measurement and Numerical Analysis. Journal of Structural Engineering, ASCE, 137(1): 143-155.

Marian, L. & Giaralis, A. (2013) Optimal design of inerter devices combined with TMDs for vibration control of buildings exposed to stochastic seismic excitations. In: Proceedings of the 11th International Conference on Structural Safety and Reliability for Integrating Structural Analysis, Risk and Reliability-ICOSSAR2013, New York, 137, 1025-1032.

Marian, L. & Giaralis, A. (2014). Optimal design of a novel tuned mass-damper–inerter (TMDI) passive vibration control configuration for stochastically support-excited structural systems. Probabilistic Engineering Mechanics, 38, 156–164. https://doi.org/10.1016/j.probengmech.2014.03.007

Matta, E. & De Stefano, A. (2009). Seismic performance of Pendulum and translational roof-garden TMDs. Mechanical Systems and Signal Processing, 23(3), 908–921. https://doi.org/10.1016/j.ymssp.2008.07.007

Mitseas, I.P., Kougioumtzoglou, I.A., Giaralis, A. & Beer, M. (2018). A novel stochastic linearization framework for seismic demand estimation of hysteretic MDOF systems subject to linear response spectra. Structural Safety, 72, 84-98.

Naeim, F.,& Kelly, J. M. (1999). Design of seismic isolated structures. https://doi.org/10.1002/9780470172742

Nagarajaiah, S. & Xiaohong, S. (2000). Response of base-isolated USC hospital building in Northridge earthquake, Journal of Structural Engineering, 126(10), 1177–1186.

Nakamura, Y., Fukukita, A., Tamura, K., Yamazaki, I., Matsuoka, T., Hiramoto, K. & Sunakoda, K. (2014). Seismic response control using electromagnetic inertial mass dampers. Earthquake Engineering & Structural Dynamics, 43(4), 507–27.

Nakaminami, S., Kida, H., Ikago, K. & Inoue N. (2017). Dynamic testing of a full-scale hydraulic inerter-damper for the seismic protection of civil structures. 7th International conference on advances in experimental structural engineering, (pp. 41–54). DOI: 10.7414/7aese.T1.55.2016.

Ohtori, Y., Christenson, R. E., Spencer, B. F. & Dyke, S. J. (2004). Benchmark control problems for seismically excited nonlinear buildings. Journal of Engineering Mechanics, 130(4), 366–385. https://doi.org/10.1061/(asce)0733-9399(2004)130:4(366)

Patsialis, D., Taflanidis, A.A. & Giaralis, A. (2021). Tuned-mass-damper-inerter optimal design and performance assessment for multi-storey hysteretic buildings under seismic excitation. Bulletin of Earthquake Engineering, DOI: 10.1007/s10518-021-01236-4.

Pietrosanti, D., De Angelis, M. & Basili, M. (2017). Optimal design and performance evaluation of systems with Tuned Mass Damper Inerter (TMDI). Earthquake Engineering & Structural Dynamics, 46(8), 1367–1388. https://doi.org/10.1002/eqe.2861

Pietrosanti, D., De Angelis, M. & Basili, M. (2020). A generalized 2-DOF model for optimal design of MDOF structures controlled by Tuned Mass Damper inerter (TMDI). International Journal of Mechanical Sciences, 185, 105849. https://doi.org/10.1016/j.ijmecsci.2020.105849

Pietrosanti, D., De Angelis, M. & Giaralis, A. (2021). Experimental seismic performance assessment and numerical modelling of nonlinear inerter Vibration absorber (iva)-equipped base isolated structures tested on shaking table. Earthquake Engineering & Structural Dynamics, 50(10), 2732–2753. https://doi.org/10.1002/eqe.3469

Rajana, K. Wang, Z. & Giaralis, A. (2023). Optimal design and assessment of tuned mass damper inerter with nonlinear viscous damper in seismically excited multi-storey buildings. Bulletin of Earthquake Engineering, 21, 1509-1539.

Rana R. & Soong, T.T. (1998). Parametric study and simplified design of Tuned Mass dampers. Engineering Structures, 20(3), 193–204. https://doi.org/10.1016/s0141-0296(97)00078-3

Roberts, J. & Spanos, P. (2003). Random vibration and statistical linearization. Dover Publications.

Ruiz, R., Taflanidis, A., Giaralis, A. & Lopez-Garcia, D. (2018). Risk-informed optimization of the tuned mass-damper-inerter (TMDI) for the seismic protection of multi-storey building structures. Engineering Structures, 177, 836-850.

Ryan, K. L. & Earl, C. L. (2010). Analysis and design of inter-story isolation systems with nonlinear devices. Journal of Earthquake Engineering, 14(7), 1044–1062. https://doi.org/10.1080/13632461003668020

Sgobba, S. & Marano, G. C. (2010). Optimum design of linear tuned mass dampers for structures with nonlinear behaviour. Mechanical Systems and Signal Processing, 24(6), 1739–1755. https://doi.org/10.1016/j.ymssp.2010.01.009

Smith, M. C. (2002). Synthesis of mechanical networks: The inerter. IEEE Transactions on Automatic Control, 47(10), 1648–1662. https://doi.org/10.1109/tac.2002.803532

Smith, M. C. (2020). The inerter: A retrospective. Annual Review of Control, Robotics, and Autonomous Systems, 3(1), 361–391. https://doi.org/10.1146/annurev-control-053018-023917

Soto, M.G. & Adeli, H. (2013) Tuned mass dampers. Archives in Computational Methods in Engineering 20, 419–431.

Spanos, P.D., Giaralis, A. & Politis, N.P. (2007). Time- frequency representation of earthquake accelerograms and inelastic structural response records using the adaptive chirplet decomposition and empirical mode decomposition. Soil Dynamics and Earthquake Engineering, 27: 675- 689.

Spanos, P.D. & Giaralis, A. (2013). Third-order statistical linearization-based approach to derive equivalent linear properties of bilinear hysteretic systems for seismic response spectrum analysis. Structural Safety, 44, 59-69.

Taflanidis, A., Giaralis, A. & Patsialis, D. (2019). Multi-objective optimal design of inerter-based vibration absorbers for earthquake protection of multi-storey building structures. Journal of the Franklin Institute, 356(14), 7754-7784. https://doi.org/10.1016/j.jfranklin.2019.02.022

Tsiatas, G.C. & Karatzia, D.A. (2020). Reliability analysis of the Hysteretic Nonlinear Energy Sink in shock mitigation considering uncertainties. Journal of Vibration and Control, 26(23-24): 2261-2273.

Tsiatas, G.C., Charalampakis, A.E. & Tsopelas, P. (2020). A comparative study of linear and nonlinear mass damping systems under seismic excitation. Engineering Structures, 219: 110926.

Uang, C. & Bertero, V. (1988). Use of energy as a design criterion in earthquake-resistant design. Technical Report UCB/EERC 88-18, Earthquake Engineering Research Center, University of California at Berkeley.

Vakakis, A.F. & Gendelman, O. (2001). Energy pumping in nonlinear mechanical oscillators: part II-resonance capture. Journal of Applied Mechanics, 68(1): 42–48.

Villaverde, R. (1998). Roof isolation system to reduce the seismic response of buildings: A preliminary assessment. Earthquake Spectra, 14(3): 521-532.

Villaverde, R. & Mosqueda, G. (1999). Aseismic roof isolation system: Analytic and shake table studies. Earthquake Engineering & Structural Dynamics, 28(3), 217–234. https://doi.org/10.1002/(sici)1096-9845(199903)28:3<217::aid-eqe813>3.0.co;2-g

Villaverde, R. (2002). Aseismic roof isolation system: Feasibility Study with 13-story building. Journal of Structural Engineering, 128(2), 188–196. https://doi.org/10.1061/(asce)0733-9445(2002)128:2(188)

Wang, Z. & Giaralis, A. (2021). Top-story softening for enhanced mitigation of vortex shedding-induced vibrations in wind-excited tuned mass damper inerter-equipped tall buildings. Journal of Structural Engineering, 147(1). https://doi.org/10.1061/(asce)st.1943-541x.0002838

Warn, G.P. & Ryan, K.L. (2012). A review of seismic isolation for buildings: historical development and research needs. Buildings 2, 300–325.

Wen, Y.-K. (1976). Method for random vibration of Hysteretic Systems. Journal of the Engineering Mechanics Division, 102(2), 249–263. https://doi.org/10.1061/jmcea3.0002106

Wen, Y. K. (1980). Equivalent linearization for hysteretic systems under random excitation. Journal of Applied Mechanics, 47(1), 150–154. https://doi.org/10.1115/1.3153594

Whittle, J.K., Williams, M.S., Karavasilis, T.L. & Blakeborough, A. (2012). A comparison of viscous damper placement methods for improving seismic building design. Journal of Earthquake Engineering 16, 540-560.

Wolff, E.D., Ipek, C., Constantinou, M.C. & Tapan, M. (2015) Effect of viscous damping devices on the response of seismically isolated structures. Earthquake Engineering & Structyral Dynamis 44, 185-198.

Xie, Q. (2005). State of the art of buckling-restrained braces in Asia, Journal of Constructional Steel Research. 61, 727–748. https://doi.org/10.1016/j.jcsr.2004.11.005.

Zemp, R., De la Llera, J.C. & Roschke, P. (2011). Tall building vibration control using a TM-MR damper assembly: Experimental results and implementation. Earthquake Engineering & Structural Dynamics, 40, 257–271.